Title
SURFACE AND CURVATURE PROPERTIES OF NEUTRON-RICH NUCLEI

Author
Kolehmainen, K.

Publication Date
1984-11-01

Lawrence Berkeley Laboratory
UNIVERSITY OF CALIFORNIA

Submitted to Nuclear Physics A

SURFACE AND CURVATURE PROPERTIES OF
NEUTRON-RICH NUCLEI

K. Kolehmainen, M. Prakash,
J.M. Lattimer, and J.R. Treiner

November 1984

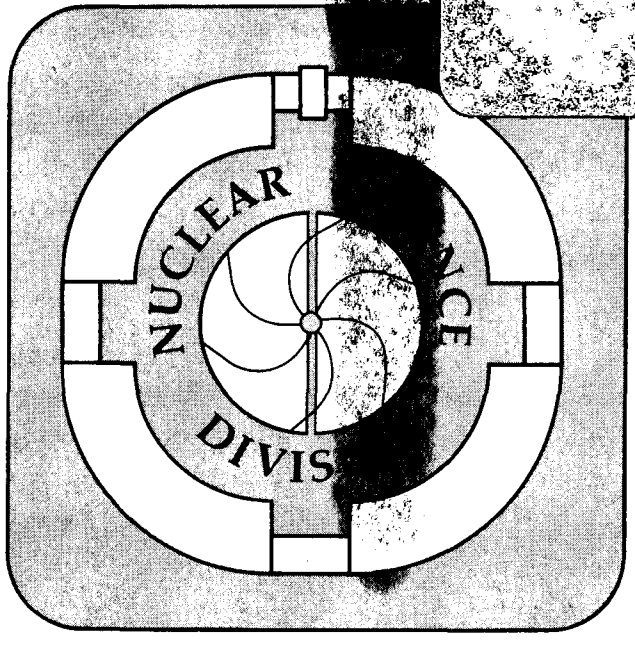

Prepared for the U.S. Department of Energy under Contract DE-AC03-76SF00098

DISCLAIMER

SURFACE AND CURVATURE PROPERTIES OF NEUTRON-RICH NUCLEI

KAREN KOLEHMAINEN[1]

Nuclear Science Division, 70A-3307, Lawrence Berkeley Laboratory, Berkeley, CA 94720, USA

MADAPPA PRAKASH[2]

Department of Physics, State University of New York at Stony Brook, Stony Brook, NY 11794, USA

JAMES M. LATTIMER[3]

Department of Earth and Space Sciences, State University of New York at Stony Brook, Stony Brook, NY 11794, USA

and

JACQUES R. TREINER[4]

Nuclear Science Division, 70A-3307, Lawrence Berkeley Laboratory, Berkeley, CA 94720, USA

[1] Supported in part by the US Department of Energy under contract DE-AC03-76SF00098 with Lawrence Berkeley Laboratory.

[2] Supported in part by the US Department of Energy under contract DE-AC02-76ER13001 with the State University of New York at Stony Brook.

[3] Alfred P. Sloan Foundation Fellow

[4] On leave from Institut de Physique Nucleaire, BP no.1, 91406 Orsay, Cedex, France

ABSTRACT

We use the extended Thomas-Fermi approximation and Skyrme-type interactions to describe the energy density of a semi-infinite slab of neutron-rich nuclear matter at zero temperature. We allow for the existence of a drip phase at low proton fractions in addition to the more dense nuclear phase. We determine various bulk properties of both phases when the system is in equilibrium. We extend the usual definition of the surface energy to apply to the case where drip is present. Assuming the density profile has the form of a Fermi function to a power, we perform a constrained variational calculation to determine the parameters of the density profile. The surface and curvature energies are calculated for proton fractions ranging from 0.5 (symmetric nuclear matter) to zero (pure neutron matter) for typical Skyrme-type interactions. We find significantly different asymmetry dependences for different interactions. For proton fractions close to 0.5, our results are in close agreement with the predictions of the droplet model. We also present results of calculations for fission barrier properties and phase transitions between nuclei and bubbles to highlight the role of surface and curvature energies in the neutron rich regime.

1. INTRODUCTION

Many problems in nuclear physics and astrophysics can be most easily approached by using a simple description of the properties of nuclei and dense matter. One approach is to write the total energy of a nucleus with Z protons and A-Z neutrons as the sum of volume (v), surface (s), curvature (c), and Coulomb (Coul) terms, as in the standard liquid drop model:

$$E_{tot} = E_v + E_s + E_c + E_{Coul}$$

$$= a_v A + a_s A^{2/3} + a_c A^{1/3} + a_{Coul} x^2 A^{5/3} \quad , \tag{1.1}$$

where $x = Z/A$. The surface and curvature properties play a particularly important role in the description of many physical phenomena, as outlined below. Our purpose here is to present a simple description of surface and curvature properties which reproduces closely the results of more exact but time consuming calculations. We then use it to calculate surface and curvature properties for a wide range of values of x (0.5 to zero), and for several effective interactions.

In describing neutron stars[1] and supernovae,[2-4] it is important to determine equilibrium sizes of nuclei, electron capture rates,[5] and level densities,[6] all of which are sensitive to surface and curvature properties. Another important astrophysical application is the phase transition[7] between nuclei and bubbles. Similarly, liquid-gas phase transitions may occur in heavy-ion collisions. Surface and curvature energies are instrumental in determining the distribution of sizes of fragments which are emitted from the

expanding collision region for temperatures less than the critical temperature.[8] Surface and curvature energies are crucial in calculating fission barrier heights and shapes of saddle point configurations.[40] An analysis of the sensitivity of the results (in the applications mentioned above) on the quantitative aspects of the surface properties is given in ref. 9.

Most calculations of surface properties have been done for proton fractions corresponding to laboratory nuclei, i.e., for x = 0.4 to 0.5. In astrophysical applications, we need to consider a larger range of proton fractions. In addition, the existence of the drip phase must be taken into account. If x is less than about 0.34, neutrons are no longer bound in nuclei. In the outer regions of neutron stars and certain stages in the evolution of supernova cores, nuclei are confined in a lattice and the drip neutrons occupy the spaces in between[1]. Protons do not drip until x is about 0.04 at zero temperature.[10] At finite T, both neutrons and protons can drip at much larger proton fractions than at T = 0.[10] In this work, we will consider only the zero temperature case.

Our approach is to describe both nuclear and drip phases using the energy density functional formalism.[11] Skyrme-type interactions[12] are used to give the effective potential. We use the Thomas-Fermi (TF) approximation with corrections aimed at reproducing realistic kinetic energy densities. Minimizing the energy with respect to variations in the density results in a set of Euler-Lagrange equations. The solution of these highly non-linear coupled differential equations constitutes the exact variational method. Another approach is to assume specific forms for both neutron and proton density distributions and minimize the energy with respect to the parameters of the forms assumed. The resulting set of equations can then be solved to

find the density distribution. This restricted variational method has been shown to be a good approximation by several authors,[13-15] who demonstrate that the energy obtained in this manner is close to that obtained in the exact variational method. We will adopt the restricted variational method for the sake of simplicity. Specifically, we assume that both neutron and proton distributions have the form of a Fermi function to a power. In the case where drip is present, this is modified to a constant plus a Fermi function to a power.

The determination of the surface properties is most easily done by considering a leptodermous expansion[18] of a finite nucleus. The geometry reduces to that of a semi-infinite slab of nuclear matter, separated by a plane interface from either vacuum or drip matter, depending on the proton fraction of the nuclear matter. We generalize this approach to asymmetric nuclear matter and to include the drip phase. It is straightforward to show[16-18] that the curvature energy may be simply extracted from the semi-infinite slab surface calculation. For realistic nuclei, the contribution of the curvature energy to the total is not insignificant.

Results for $a_{s,c}$ obtained from semi-infinite slab calculations are very useful in that they may be used to explore the sensitivity to the underlying nucleon-nucleon interaction. The constants $a_{s,c}$ in eq. (1.1), however, refer to a finite nucleus, and are not the same as those for a slab. Several corrections to the slab results have to be considered before using eq. (1.1) to calculate the energy of a finite nucleus. For small asymmetries, these corrections are usually calculated by expanding the total energy in terms of deviations from results for symmetric matter. For effective forces with relatively large incompressibilities, only the first term in the expansion need be considered. This situation changes for forces with relatively

smaller incompressibilities where higher order terms have to be retained.[14,42] In presenting our results for the applications considered in this paper, we have, however, used the lowest order corrections only. Therefore, our results for the nuclear physics application differ slightly from the more exact results; the qualitative aspects are, however, trustworthy. For the astrophysical application, our results may be considered quantitative since the nuclear sizes involved are very large.

In section 2, we present the conditions for bulk equilibrium between the nuclear and drip regions. In sect. 3, we present formulae for the surface and curvature energies in the general case with neutron drip. We describe the determination of surface properties by assuming Fermi functions to powers for the neutron and proton distributions in sect. 4. Section 5 contains a brief discussion of the Thomas-Fermi method and corrections to it. Results are given in sect. 6, where we also include comparisons with the results of more exact methods. In sect. 7, our results for surface and curvature energies are used in the calculation of fission barriers and the description of phase transitions between nuclei and bubbles. Our conclusions are given in sect. 8.

2. DETERMINATION OF BULK EQUILIBRIUM

For matter at proton density ρ_p, neutron density ρ_n, and total density $\rho = \rho_p + \rho_n$, Skyrme-type interactions lead to an energy per unit volume of[19]

$$\begin{aligned}\epsilon(\rho_n,\rho_p) &= (\hbar^2/2m)\tau + \tfrac{1}{2}t_0(1+\tfrac{1}{2}x_0)\rho^2 + \tfrac{1}{12}t_3(1+\tfrac{1}{2}x_3)\rho^{\gamma+2} \\ &\quad - \tfrac{1}{2}(\rho_n^2+\rho_p^2)[t_0(\tfrac{1}{2}+x_0) + \tfrac{1}{6}t_3\rho^\gamma(\tfrac{1}{2}+x_3)] \\ &\quad + \tfrac{1}{4}\rho\tau[t_1(1+\tfrac{1}{2}x_1)+t_2(1+\tfrac{1}{2}x_2)] + \tfrac{1}{4}(\rho_n\tau_n+\rho_p\tau_p)[t_2(\tfrac{1}{2}+x_2)-t_1(\tfrac{1}{2}+x_1)] \\ &\quad - \tfrac{1}{16}(\nabla\rho)^2[t_2(1+\tfrac{1}{2}x_2) - 3t_1(1+\tfrac{1}{2}x_1)] \\ &\quad - \tfrac{1}{16}[(\nabla\rho_n)^2+(\nabla\rho_p)^2][3t_1(\tfrac{1}{2}+x_1) + t_2(\tfrac{1}{2}+x_2)] \\ &\quad - \tfrac{1}{2}W_o[\rho\nabla\cdot\mathbf{J} + \rho_n\nabla\cdot\mathbf{J}_n + \rho_p\nabla\cdot\mathbf{J}_p] \ , \end{aligned} \tag{2.1}$$

where m is the nucleon mass, $\tau = \tau_n+\tau_p$ and $\mathbf{J} = \mathbf{J}_n+\mathbf{J}_p$. The Skyrme parameters t_0 through t_3, x_0 through x_3, γ, and W_o, are characteristics of the given interaction and are determined by fitting various properties of nuclei (also neutron matter in some cases). Table 1 gives values of these parameters for the interactions we have investigated. For the kinetic energy densities τ_n and τ_p, we use the extended Thomas-Fermi (ETF + SO) result

$$\tau_i = \tfrac{3}{5}(3\pi^2)^{2/3}\rho_i^{5/3} + \eta_1(\nabla\rho_i)^2/\rho_i + \eta_2\nabla^2\rho_i + \mathbf{J}_i^2/2\rho_i \ , \tag{2.2}$$

where i denotes n or p. The coefficients η_1 and η_2 are constants whose values we will discuss later, and the spin density $\mathbf{J}_i$ is

$$\mathbf{J}_i = -(2m_i^*/\hbar^2)W_o\rho_i(\nabla\rho_i + \tfrac{1}{2}\nabla\rho_j) \ , \tag{2.3}$$

where m_i^* is the nucleon effective mass, defined in eq. (2.6). The last terms in eqs. (2.1) and (2.2) arise due to the spin-orbit (SO) interaction. We will present results for the full ETF + SO case and the Thomas-Fermi case, in which $\eta_1 = \eta_2 = W_o = 0$.

The expression (2.1) is used to describe matter in both the nuclear and drip regions. Sufficiently far from the plane interface in either direction, the density becomes a constant, and we can drop the derivative terms in writing $\epsilon_o = \epsilon(\rho_o)$, the energy density far inside the nuclear region, and $\epsilon_d = \epsilon(\rho_d)$, the energy density far inside the drip region, where $\rho_o = \rho_{po} + \rho_{no}$ and $\rho_d = \rho_{pd} + \rho_{nd}$. The bulk energy per particle far inside the nuclear region, $a_V = \epsilon_o/\rho_o \sim -16$ MeV for symmetric matter at saturation density. A corresponding expression gives the energy per particle in the drip region.

The chemical potential μ_{ir}, where i is n or p, and r is used to designate either the nuclear phase (o) or the drip phase (d), is given by

$$\mu_{ir} = (d\epsilon/d\rho_i)|_{jr} = (\partial\epsilon/\partial\rho_i)|_{jr} + (\partial\epsilon/\partial\tau_i)|_{jr}(d\tau_i/d\rho_i)|_{jr} , \qquad (2.4)$$

where $j \neq i$. The notation $|_{jr}$ means keep ρ_j fixed, and evaluate the expression in the region r. We can rewrite eq. (2.4) as

$$\mu_{ir} = (\hbar^2/2m^*_{ir})(3\pi^2)^{2/3}\rho_{ir}^{2/3} + V_{ir} , \qquad (2.5)$$

where the effective mass m_i^* is given by

$$\hbar^2/2m_i^* = \partial\epsilon/\partial\tau_i , \qquad (2.6)$$

and the single particle potential V_i is $\partial\epsilon/\partial\rho_i$. The pressure is found to be

$$P_r = \rho_r (d\epsilon/d\rho)\big|_r - \epsilon_r = \mu_{pr}\rho_{pr} + \mu_{nr}\rho_{nr} - \epsilon_r \ , \tag{2.7}$$

and the bulk incompressibility K_r is given by

$$K_r = 9(dP/d\rho)\big|_r \ . \tag{2.8}$$

When no drip particles are present, the pressure of the material in the nuclear region must be zero in equilibrium. This condition is sufficient to determine the nuclear density for a specified x, and is equivalent to minimizing the bulk energy per particle, a_v, with respect to ρ_o. This is the usual saturation condition. When drip particles are present, we must determine ρ_{no}, ρ_{po}, ρ_{nd}, and ρ_{pd}. The choice of the proton fraction in the nuclear region fixes one of these, and the other three are fixed by the equality of the pressure and proton and neutron chemical potentials in the two phases. One should note that if we were considering a finite spherical nucleus rather than a slab, the pressure equilibrium equation would contain extra terms due to the pressure on the interior of the nucleus caused by the surface tension and the Coulomb forces. To find the density and proton fraction at points near the interface, i.e., to find the overall density profile, one must consider the effects of the surface.

3. DEFINITION OF THE SURFACE AND CURVATURE ENERGIES

For a finite spherical nucleus surrounded by drip particles, the total energy is given by

$$E_{tot} = \int_0^{\Psi} \epsilon(\rho)\ 4\pi r^2 dr\ , \tag{3.1}$$

where we will later take the limit $\Psi \to \infty$. Letting Λ be an as yet arbitrary radius of the nucleus, this may be rewritten as

$$E_{tot} = 4\pi\{\epsilon_o \Lambda^3/3 + (\Psi^3 - \Lambda^3)\epsilon_d/3 + \Sigma/4\pi + (\epsilon_o - \epsilon_d)[\int_0^{\Lambda} r^2(\rho-\rho_o)\ dr + \int_{\Lambda}^{\Psi} r^2(\rho-\rho_d)\ dr]/(\rho_o-\rho_d)\}\ , \tag{3.2}$$

where

$$\Sigma = 4\pi\int_0^{\Psi} r^2\ \chi\ dr\ , \tag{3.3}$$

and

$$\chi = \epsilon - \epsilon_o(\rho-\rho_d)/(\rho_o-\rho_d) + \epsilon_d(\rho-\rho_o)/(\rho_o-\rho_d)\ . \tag{3.4}$$

Note that Σ is independent of Λ. Similarly, we may write the total number of nucleons as

$$A_{tot} = 4\pi\int_0^{\Psi} r^2\rho\ dr = 4\pi\{\rho_o\Lambda^3/3 + \rho_d(\Psi^3 - \Lambda^3)/3 - \int_0^{\Lambda} r^2(\rho_o-\rho)\ dr + \int_{\Lambda}^{\Psi} r^2(\rho-\rho_d)\ dr\}\ . \tag{3.5}$$

A simple choice for Λ is the value R for which the final two integrals in eqs. (3.2) and (3.5) vanish. The radius R has the physical significance that a 'reference' density distribution, with constant density ρ_o from r = 0 to r = R, and constant density ρ_d outside of r = R, contains the same total number of particles as the actual density distribution. We can define equivalent neutron and proton radii, R_n or R_p, in an analogous fashion:

$$N_{i,tot} = (4\pi/3)\ [\rho_{io} R_i^{\,3} + \rho_{id}(\Psi^3 - R_i^{\,3})]\ , \tag{3.6}$$

where i denotes n or p. Comparing eqs. (3.5) and (3.6), we see that R, R_n, and R_p are related by

$$R^3(\rho_o - \rho_d) = R_n^{\,3}(\rho_{no} - \rho_{nd}) + R_p^{\,3}(\rho_{po} - \rho_{pd})\ . \tag{3.7}$$

With R as the choice of radius, the surface and curvature energies, defined as the difference between the total and bulk energies, are then given by

$$E_{tot} - E_{b,R} = E_{s,R} + E_{c,R} = \Sigma\ , \tag{3.8}$$

where the subscript R indicates energies with respect to the radius R. From eq. (3.4), we note that $\chi \to 0$ as $\rho \to \rho_o$ or $\rho \to \rho_d$. For large nuclei, the region over which the density falls from ρ_o to ρ_d is small compared to R. Therefore contributions to Σ from outside this surface region are negligible, and we can replace r^2 by $R^2 + 2R(r-R)$ in eq. (3.3) since the integral is non-zero only for $r-R \ll R$. With exponentially small terms dropped, we can also extend the lower limit of the integral to $-\infty$ and the upper limit to $+\infty$. We thus obtain

$$\Sigma = 4\pi R^2 \int_{-\infty}^{\infty} \chi \, dr + 8\pi R \int_{-\infty}^{\infty} (r-R)\chi \, dr \ . \tag{3.9}$$

In the following we make further refinements so that the two contributions to Σ may be evaluated using the features of a slab geometry.[16-18] For a large nucleus, the mean curvature $k = 2/R$ is small; this fact may be utilized to expand the integrals in eq. (3.9) in k around k = 0. Keeping terms of order R and larger, and identifying terms of order R^2 as the surface energy and terms of order R as the curvature energy, we obtain

$$E_{s,R} = 4\pi R^2 \, \sigma_{s,R} = 4\pi R^2 [\int_{-\infty}^{\infty} \chi \, dz]_{k=0} \tag{3.10}$$

and

$$E_{c,R} = 8\pi R \, \sigma_{c,R} = 8\pi R [\int_{-\infty}^{\infty} (z-R)\chi \, dz + \int_{-\infty}^{\infty} \partial\chi/\partial k \, dz]_{k=0} \ , \tag{3.11}$$

where χ is given by eq. (3.4). The subscript R emphasizes the fact that the energies depend on one's choice of surface position, here equal to R. The surface energy per unit area is denoted by σ_s, and the curvature energy per unit length is denoted by σ_c. Note that since all terms are evaluated at k = 0, the finite nucleus has been replaced by a semi-infinite slab, which we have emphasized by replacing r by the Cartesian coordinate z. In appendix A, we discuss the relative contributions of the two terms for the curvature energy in eq. (3.11), when χ is calculated using the Skyrme energy density in eq. (2.1). From the results of this appendix, we note that it is always possible to rewrite the energy density in such a way that the last term in eq. (3.11) vanishes.

The definitions given in eqs. (3.10) and (3.11) satisfy two conditions which must be required of any definition of the surface or curvature energy. One is that they vanish as $\rho_d \to \rho_o$, i.e., as the system becomes uniform and therefore has no surface. Secondly, they should be unchanged if ρ_o and ρ_d are interchanged, since we can set up the coordinate system with either region on either side.[1]

For the slab geometry an equation similar to (3.7) may be obtained relating R, R_n and R_p. As in the finite nucleus case, the equivalent matter radius R (or location) is defined so that the true density profile and a squared-off density profile have the same total number of particles, i.e.,

$$\int_{R_1}^{R_2} \rho dz = \rho_o(R - R_1) + \rho_d(R_2 - R) \ , \tag{3.12}$$

where R_1 and R_2 are sufficiently far inside the nuclear and drip regions, respectively, for the density to have attained its appropriate asymptotic value. Analogous definitions for R_n and R_p are obvious. We thus obtain

$$R(\rho_o - \rho_d) = R_n(\rho_{no} - \rho_{nd}) + R_p(\rho_{po} - \rho_{pd}) \ , \tag{3.13}$$

up to order R^{-2}. This equation may also be derived from the finite nucleus result, eq. (3.7), in a straightforward manner.

****

1./Von Groote[20] also considers the problem of defining the surface energy when drip is present. Instead of defining R as we have in eq. (3.7), though, he uses the same definition of R as when there is no drip, although the expressions for R_n and R_p are modified to include drip. As a result, his expression for the surface energy, when compared to our eq. (3.10), contains an extra factor of ρ_d/ρ_o in the last term of χ. Von Groote's definition does not satisfy the requirement of being symmetric with respect to the nuclear and drip phases, and is therefore inappropriate.

While the choice of radius does not alter the total energy, it will affect the values of the surface and curvature energies since the bulk energy E_b depends on this radius. If we choose the radius as R_p, as is done in the compressible liquid drop model of Lamb et al.,[22] we find

$$E_{s,p}/4\pi R_p^2 = \sigma_{s,p} = \int_{-\infty}^{\infty} \chi \, dz + (R_n - R_p)(\epsilon_o - \epsilon_d)(\rho_{no} - \rho_{nd})/(\rho_o - \rho_d) \qquad (3.14)$$

and

$$E_{c,p}/8\pi R_p = \sigma_{c,p} = \int_{-\infty}^{\infty} \chi(z - R_p)dz + \frac{1}{2}(R_n - R_p)^2(\epsilon_o - \epsilon_d)(\rho_{no} - \rho_{nd})/(\rho_o - \rho_d) \qquad (3.15)$$

Similiar expressions for $E_{s,n}$ and $E_{c,n}$ can be found by interchanging n and p in the above equations. These definitions satisfy our two conditions, but introduce an asymmetry in the way neutrons and protons are treated. However, since the Coulomb energy is usually expressed in terms of R_p, it is desirable to use $E_{s,p}$ and $E_{c,p}$ in some situations. Since $\epsilon_o - \epsilon_d$ is always negative (i.e., the drip material is less bound than the nuclear material), $\sigma_{s,p} < \sigma_{s,R} < \sigma_{s,n}$ and $\sigma_{c,p} < \sigma_{c,R} < \sigma_{c,n}$.

A more convenient thermodynamic energy than the internal energy is the thermodynamic potential $\Omega_{tot} = E_{tot} - \mu_n N_n - \mu_p N_p$. It is straightforward to show that $\Omega_s + \Omega_c$ does <u>not</u> depend on one's choice of nuclear radius. In many applications, such as in the equation of state of Lamb et al.,[22] it is the thermodynamic potential that is of utility. As with the internal energy, we define for a finite nucleus,

$$\Omega_s + \Omega_c = \Omega_{tot} - \Omega_b \, , \qquad (3.16)$$

where $\Omega_b = -PV = -4\pi\Psi^3 P/3$. The nuclear matter inside the nucleus is in pressure equilibrium with its surroundings, so we have

$$P = \epsilon_o - \mu_n\rho_{no} - \mu_p\rho_{po} = \epsilon_d - \mu_n\rho_{nd} - \mu_p\rho_{pd} \ . \tag{3.17}$$

Since neither Ω_{tot} nor Ω_b depends on the nuclear radius, however defined, unlike the case for E_b, it is clear that $\Omega_s+\Omega_c$ also does not depend on the radius. It is easy to show that for a finite nucleus,

$$\Omega_s + \Omega_c = \Sigma - (4\pi/3)(R_n^3-R_p^3)(\rho_{no}-\rho_{nd})(\rho_{po}-\rho_{pd})(\mu_n-\mu_p)/(\rho_o-\rho_d) . \tag{3.18}$$

For the slab geometry, we have

$$\Omega_s/4\pi\Lambda^2 = \omega_s = \int_{-\infty}^{\infty} \chi dz - (R_n-R_p)(\rho_{no}-\rho_{nd})(\rho_{po}-\rho_{pd})(\mu_n-\mu_p)/(\rho_o-\rho_d) \tag{3.19}$$

and

$$\Omega_c/8\pi\Lambda = \omega_{c,\Lambda} = \int_{-\infty}^{\infty} (z-\Lambda)\chi \ dz$$

$$- \frac{1}{2}(R_n-R_p)^2(\rho_{no}-\rho_{nd})(\rho_{po}-\rho_{pd})(\mu_n-\mu_p)/(\rho_o-\rho_d) \tag{3.20}$$

where Λ is any radius. We have denoted the surface thermodynamic potential per unit area by ω_s and the curvature thermodynamic potential per unit length by ω_c. Thus, ω_s is independent of the radius choice, but ω_c is not. The relationship between the energy and the thermodynamic potential is also discussed in refs. 21 and 22.

The slab values of w_s, w_c, σ_s and σ_c cannot be directly applied to the liquid drop model because the bulk equilibrium conditions are somewhat modified due to Coulomb and finite-size effects. For example, eq. (3.17) would contain an extra term due to the compression of the nucleus by the surface tension. Therefore, one should exercise caution before using these results with the standard liquid drop model (which is an expansion in A alone) without modification. (For a discussion of the lowest order corrections in the droplet model, see section 6E.) However, in the compressible liquid drop model[22], which explicitly contains the effects due to the difference of ρ_o from the saturation value, the modifications involve only a small, simple correction in μ_n and may often be ignored (see the example in section 7B).

We have not yet assumed any form for the density distribution, and hence the relations given here are generally valid. They can therefore be used in the exact variational problem as well as in the restricted variation. They are also valid for energy densities other than those given by the Skyrme interactions.

4. SURFACE PROPERTIES WITH FERMI FUNCTION SHAPES

It has been shown[16] that, in order to calculate terms up to order $1/R^2$ relative to the bulk energy, it is sufficient to know the neutron and proton density profiles only to order 1/R. That is, the profiles calculated in determining the surface energy are sufficient to also find the curvature energy. In general, the minimization of the total energy produces two equations for the profiles, which to lowest order are

$$\sum_{ij} Q_{ij}(\nabla\rho_i)(\nabla\rho_j) = d\epsilon_b/d\rho_i - \mu_i \ , \tag{4.1}$$

where ϵ_b is the bulk part of the Hamiltonian density. The matrix Q_{ij} consists of the coefficients of the $\nabla\rho_i\nabla\rho_j$ terms in the Hamiltonian (eq. 2.1). Instead of solving the minimization equations directly, we approximate the exact profile in terms of a Fermi function to a power. This choice has been shown to give reliable results for both surface energies and diffusenesses.[13-15] Specifically, we use

$$\rho_i(z) = \rho_{id} + (\rho_{io} - \rho_{id})\ f_i^{p_i} \ , \tag{4.2}$$

where the density is chosen to vary along the z axis, and f_i is the Fermi function

$$f_i(z) = \{1 + \exp[(z-z_i)/a_i]\}^{-1} \ . \tag{4.3}$$

We determine the diffuseness parameters a_n and a_p, the powers p_n and p_p, and the neutron skin thickness $z_n - z_p$ by minimizing the total energy with respect to them. We are allowed to choose the coordinate system so as to specify either z_n or z_p due to the translational invariance of eq. (4.1).

The minimization of the total energy is done subject to the constraint that the total numbers of both neutrons and protons remain fixed. Thus, we minimize $\Omega_{tot} = E_{tot} - \mu_n N_n - \mu_p N_p$. Minimization with respect to the diffusenesses a_i leads to

$$\frac{\partial \Omega_{tot}}{\partial a_i} = \frac{\partial \Omega_s}{\partial a_i} = \int_{-\infty}^{\infty} \frac{\partial \chi}{\partial a_i}\, dz + \frac{(\rho_{i0}-\rho_{id})(\rho_{j0}-\rho_{jd})}{(\rho_0-\rho_d)}(\mu_i-\mu_j)\frac{p_i}{a_i} \cdot \int_{-\infty}^{\infty} f_i^{p_i-1} \frac{df_i}{dz}(z-z_i)\, dz = 0, \tag{4.4}$$

for the slab geometry, where we have used eqs. (3.16) and (3.19). Similarly, minimization with respect to the powers p_i results in

$$\frac{\partial \Omega_{tot}}{\partial p_i} = \frac{\partial \Omega_s}{\partial p_i} = \int_{-\infty}^{\infty} \frac{\partial \chi}{\partial p_i} dz - \frac{(\rho_{i0}-\rho_{id})(\rho_{j0}-\rho_{jd})}{(\rho_0-\rho_d)}(\mu_i-\mu_j) \int_{-\infty}^{\infty} f_i^{p_i} \ln f_i = 0, \tag{4.5}$$

and minimization with respect to $(z_n - z_p)$ leads to

$$\frac{\partial \Omega_{tot}}{\partial (z_n-z_p)} = \frac{\partial \Omega_s}{\partial (z_n-z_p)} = \int_{-\infty}^{\infty} \frac{\partial \chi}{\partial (z_n-z_p)}\, dz - \frac{2(\rho_{n0}-\rho_{nd})(\rho_{p0}-\rho_{pd})}{(\rho_0-\rho_d)}(\mu_n-\mu_p) = 0 \tag{4.6}$$

where χ is given by eq. (3.4). The five expressions, eqs. (4.4), (4.5) and (4.6), form a set of coupled non-linear equations, which can be solved to obtain a_n, a_p, p_n, p_p, and $z_n - z_p$. With the optimum values of these

parameters, we obtain the complete density profiles; the surface and curvature energies can then be calculated using the formulae in sect. 3.

5. THE KINETIC ENERGY FUNCTIONAL

In order to apply the energy density formalism, one must have a relationship between the kinetic energy density τ and the matter density ρ. One way of obtaining such a relationship is to write the energy density as a semiclassical expansion[23] in powers of $\hbar$. The Thomas-Fermi approximation results from considering only the first (zeroth-order) term in this expansion. It is hoped that the inclusion of higher order terms (extended TF or ETF) provides systematic corrections.

The effects of including these corrections and spin-orbit terms have been investigated by Blaizot and Grammaticos[14] for symmetric matter using some Skyrme forces. The first order correction to the TF approximation (the $\hbar^2$ term) causes a decrease of 5 to 25% in the diffusenesses a_i, although for most interactions the decrease is between 5% and 10%. The surface energy constant $a_s = E_s/A^{2/3} = 4\pi r_o^2 \sigma_s$ also decreases for most forces, and the spread in a_s for symmetric matter between forces is reduced from 9 MeV to about 2 MeV. Inclusion of spin-orbit terms in the energy density causes an additional 10% decrease in both a_s and the diffuseness a_i for all interactions. It has been found[23] (for symmetric matter) that the effect of the second order correction (the $\hbar^4$ term) is almost as large as the first order correction and comes in with the opposite sign; hence the effects of the first order correction are partially cancelled. This also remains true when spin-orbit corrections are included. The validity of this result over a larger range of asymmetry and the dependence on the interaction remain to be checked.

It has been shown,[24] however, that this semiclassical expansion is not analytic in $\hbar$. Alternatively, there exist methods which include the nonanalytic structure of the density matrix.[25] In these methods, one constructs an approximate form of the density matrix by a local linearization of the potential. The kinetic energy density τ is then obtained in terms of this approximate density matrix. It has been demonstrated,[26] however, that this local linearization approximation leads to non-negligible errors in τ in the region of the shoulder of the density distribution.

In practical calculations Campi and Stringari[27] have argued that it is more sensible to use a fit to realistic forms of τ than to use the truncated versions of the semiclassical expansion. They use gradient-type corrections to the TF approximation as in eq. (2.2), with the values of η_1 and η_2 resulting from a fit to the kinetic energy density from HF calculations. They find η_1 = 0.08 to 0.11 and η_2 = 0.3 for typical Skyrme-type forces. These are to be compared with the values of η_1 = 1/4 and η_2 = 1/3 from the work of Weizsacker[28] and the usual ETF values of η_1 = 1/36 and η_2 = 1/3 from refs. 23 and 29. The results of ref. 27 show good agreement with experimental surface diffusenesses. However, their calculated surface energies lead to fission barrier heights which do not agree as well with experiments.

Brack, et al[43] have shown that using eq. (2.2), one recovers the results obtained for the surface energy by using the semi-classical kinetic energy up to $\hbar^4$ corrections if η_1 is chosen in the range (1/36)·(1.3 to 1.5). However, the surface thickness calculated with such a small value of η_1 is lower than realistic values by about 20%. (For a discussion of the dependence of surface thickness on η_1, see appendix C.) As a compromise, Treiner and Krivine[30] have used a value of η_1 = 1/18 which reproduces the value of a_s = 18.8 MeV

found in a HF calculation by Farine et al.[31] for SIII. We find that this value of η_1 reproduces the HF results[27,38,39] for SI', SkM and SkM* forces also. In refs. 27 and 39, spin-orbit forces were neglected; a comparison with our results can be made by subtracting about 1.6 MeV from the quoted HF results for a_s (see appendix C). This value of η_1 will be used in the applications presented in sect. 7. However, in order to highlight the dependence of surface and curvature properties on η_1, we present results of calculations with several choices for this parameter. For quantitative calculations of fission barriers with $\hbar^4$ corrections with SIII, SkM and SkM* forces, we refer the reader to ref. 43.

6. RESULTS AND DISCUSSION

Using the formalism of sects. 2, 3 and 4, we have carried out calculations for the Skyrme interactions SI', SIII, SkM, and SkM*.[2] We chose these four both because they demonstrate differences which are representative of the variations between all the interactions, and because they have been widely used. Since SkM and SkM* produce similar results, the SkM results are not shown in the figures for the sake of clarity. We show results for ETF+SO with η_1=1/18 and a Fermi to a power density distribution; other cases will be discussed later.

****

2./The parameters of the interaction SI' were obtained by modifying the SI parameters[19] to fit the Siemens and Pandharipande results[32] for neutron matter (by changing only x_0 and x_3, which leaves the symmetric matter results unaltered). It is hoped that this results in better agreement with the properties of neutron-rich matter and nuclei.

A. BULK PROPERTIES

To understand the behavior of the calculated results for small proton fractions, it is instructive to relate the Skyrme parameters to those of the droplet model (DM).[18] In the DM, the bulk energy per particle is written as

$$a_v = a_{v0} + J\delta^2 + (1/2)\ K_o\epsilon^2 - L\epsilon\delta^2 + (1/2)\ K_{sym}\epsilon^2\delta^2 + (1/2)\ M\delta^4 \ , \quad (6.1)$$

for small δ. Here $\delta = (\rho_n-\rho_p)/\rho$ and $\epsilon = -1/3\ (\rho-\rho_{NM})/\rho_{NM}$, where ρ_{NM} is the saturation density for symmetric nuclear matter. Equating this expression to the Skyrme expression for the bulk energy per particle, we obtain the droplet model cofficients in terms of the Skyrme parameters:

$$J = C_{NM}\ \{1/3\ \hbar^2/2m + \rho_{NM}/24\ [t_2(4+5x_2)-3t_1x_1]\} - 1/4\ t_0(1/2+x_0)\rho_{NM}$$

$$- 1/24\ t_3(1/2+x_3)\rho_{NM}^{\gamma+1} \ , \quad (6.2)$$

$$K_o = C_{NM}\ \{-6/5\ \hbar^2/2m + 3/8\ \rho_{NM}[t_2(5+4x_2)+3t_1]\}$$

$$+ 9/16\ t_3\gamma(\gamma+1)\rho_{NM}^{\gamma+1} \ , \quad (6.3)$$

$$L = C_{NM}\ \{2/3\ \hbar^2/2m + 5/24\ \rho_{NM}[t_2(4+5x_2)-3t_1x_1]\} - 3/4\ t_0(1/2+x_0)\rho_{NM}$$

$$- 1/8\ t_3(1/2+x_3)(\gamma+1)\rho_{NM}^{\gamma+1} \ , \quad (6.4)$$

$$M = C_{NM}\ \{2/81\ \hbar^2/2m + \rho_{NM}/324\ [3t_1(1+x_1)+t_2(1-x_2)]\} \ , \quad (6.5)$$

$$K_{sym} = C_{NM} \{-2/3\ \hbar^2/2m + 5/12\ \rho_{NM}[t_2(4+5x_2)-3t_1x_1]\}$$

$$-3/8\ t_3(1/2+x_3)\gamma(\gamma+1)\rho_{NM}^{\gamma+1}\ , \qquad (6.6)$$

where $C_{NM} = (3\pi^2\rho_{NM}/2)^{2/3}$. The droplet model coefficients for SI', SIII, SkM, and SkM* are listed in table 1.

By solving the bulk equilibrium conditions presented in sect. 2, we obtain the asymptotic densities ρ_{no}, ρ_{po}, ρ_{nd} and ρ_{pd}, as well as the pressure and neutron and proton chemical potentials. The asymptotic densities are shown in fig. 1 for the interactions SI', SIII and SkM*. The nuclear density ρ_o decreases monotonically with increasing asymmetry; this fall-off is quadratic for x close to 0.5 and can be expressed in terms of the DM parameters as

$$\rho_o = \rho_{NM}\ [1 - 3L\delta_o^2/(K_o + K_{sym}\delta_o^2)]\ , \qquad (6.7)$$

where $\delta_o = (\rho_{no}-\rho_{po})/\rho_o = (1-2x)$ is the bulk asymmetry parameter. The drip density is zero until $x \approx 0.34$, and then grows until both densities are equal, at which point bulk equilibrium between two phases is no longer possible. We find that this transition occurs in the range $0.01 < x < 0.08$, depending on the interaction. The drip density is virtually all neutrons; protons start to appear in the drip region at or just before the transition to uniform matter.

The saturation density ρ_o is important in describing phase transitions between nuclei and bubbles and between bubbles and uniform matter.[7] For the interactions we have studied, the nuclear saturation density ranges from 0.14 to 0.15 fm^{-3} for $x \approx 0.3$, which is the value of interest in astrophysical situations. We discuss these phase transitions in sect. 7B.

We find that the bulk properties of the drip phase are very similar for all interactions at values of $x < 0.34$. This can be understood from the fact that in this regime, the drip density is very low and the interactions are therefore unimportant. The drip phase is then well described as a noninteracting degenerate Fermi gas.

In fig. 2, we show the incompressibility, K, at the saturation density for a given x, in the nuclear region as a function of δ_o^2. We note that there is a wide variation between interactions, with K_o for symmetric matter ranging from 200 MeV to nearly 400 MeV. The interactions SkM and SkM* agree most closely with the empirical value of 220 MeV, which is deduced from the frequency of the isoscalar nuclear breathing mode. We further note that the x dependence of the incompressibility also varies widely from interaction to interaction. In terms of the DM, we find a quadratic decrease with δ_o,

$$K(\delta_o) = K_o[1 - (6L-K_{sym})/K_o\ \delta_o^2] = K_o[1 - (6L-K_{sym})/K_o\ (1-2x)^2] , \qquad (6.8)$$

for small δ_o. The values of $(6L-K_{sym})/K_o$ are 1.272, 1.275, 1.804 and 1.988 for SI', SIII, SkM and SkM*, respectively. For the case with twice as many neutrons as protons, i.e., $\delta_o = x = 1/3$, K has the values 314, 302, 176, and 177 MeV for SI', SIII, SkM and SkM*, respectively.[3]

It should be pointed out that there is a significant density dependence in the incompressibility, and the major reason (for most interactions) it decreases with δ_o is that the saturation density, ρ_o, decreases with δ_o. If one evaluated, instead, the incompressibility for a fixed density, say ρ_{NM},

****

3./As a point of interest, we give the results for the incompressibility for the finite-range nucleon-nucleon force of Friedman and Pandharipande[45]. For small δ_o, $K \approx 238\ [1 - 1.01\ \delta_o^2]$ MeV, and for $\delta_o = 1/3$, $K \approx 212$ MeV.

the coefficient of δ_o^2 in eq. (6.8) would be $+(6L + K_{sym})/K_o$. For the interactions SkM and SkM*, this has the opposite sign of the term in (6.8), and the incompressibility at a fixed density increases with asymmetry.

B. SURFACE PROPERTIES

We now examine the results for the surface properties. The dependence of such surface properties as the surface energy, curvature energy and surface thickness on parameters of the nuclear interaction and the extended Thomas-Fermi gradient corrections is discussed in appendix C.

The surface thicknesses, a_i^{90-10}, are defined as the differences between the 90% and 10% density locations:

$$a_i^{90-10} = z[\rho_i = \rho_{id} + 0.1(\rho_{io}-\rho_{id})] - z[\rho_i = \rho_{id} + 0.9(\rho_{io}-\rho_{id})]. \quad (6.9)$$

These quantities are related to the a_i's and p_i's by

$$a_i^{90-10} = a_i \ln\{(0.1^{-1/p_i} -1)/(0.9^{-1/p_i} -1)\} . \quad (6.10)$$

The diffusenesses a_n and a_p, the powers p_n and p_p, and the 90-10 surface thicknesses a_i^{90-10} are shown as functions of δ_o in figs. 3, 4, and 5, respectively. We note that for all interactions, $a_n \sim a_p$, i.e., the difference between a_p^{90-10} and a_n^{90-10} comes mainly from the difference in the p_i's, not the a_i's. In ref. 9, where calculations are carried out with $p_i = 1$, the difference between a_n and a_p is seen to be much larger; in fact, in that case a_n and a_p (as functions of δ_o) exhibit much the same forms as a_n^{90-10} and a_p^{90-10} do in the present ($p_i \neq 1$) case. For small neutron excesses, the result $a_n = a_p$ is exact, as can be demonstrated by considering the two coupled Euler equations.[30] It is interesting to see from fig. 3 that this result is also true for small proton fractions. This indicates that it would

be a reasonable approximation to set $a_n = a_p$, thus reducing the set of minimization conditions from five to four equations.

In the density profile of eq. (4.2), the choice $p_i = 1$ (Fermi function) leads to a variation in the surface that is symmetric about $z = z_i$. When $p_i \neq 1$, an asymmetry of the surface around $z = z_i$ develops. With increasing p_i, this asymmetry is enhanced.

In fig. 6, we show our results for the neutron skin thickness, $t = R_n - R_p$. As the system becomes neutron-rich, a neutron skin develops, and hence t grows from its value of zero at x = 0.5. For small δ_o, the growth is linear in x, as predicted by the DM:

$$t = (3/2)\ r_o(J/Q)\ \delta_o\ , \tag{6.11}$$

where Q measures the stiffness of the system against pulling R_n and R_p apart. We observe that forces with large values of J/Q have thick neutron skins. This can be understood as follows: If the bulk symmetry coefficient J is large, the surface symmetry energy should also be large in order to keep the total symmetry energy (which is fixed empirically) constant (see eq. 6.17). This constraint implies that small values of Q are associated with large values of J, both tendencies contributing to increase the ratio J/Q. In other words, it costs the system a large amount of energy to produce an asymmetry in the bulk region, hence it favors putting much of its neutron excess into the surface region instead, thus creating a thick neutron skin.

We now come to our results for the surface energy. The surface energy per unit area, $\sigma_{s,R} = E_{s,R}/(4\pi R^2) = a_s/(4\pi r_o^2)$, and the thermodynamic potential per unit area ω_s are shown in fig. 7. At x= 0.5, σ_s ranges from 1.03 to 1.10 MeV fm^{-2}, corresponding to a range for $a_s = E_s/A^{2/3}$ of 17.3 to

18.8 MeV. The surface energy per unit area, $\sigma_{s,R}$, grows with the neutron skin thickness, reaching a maximum at somewhat past the neutron drip point, and then decreases to zero as we reach the transition point to a uniform medium. In general, forces with thick neutron skins also have large surface energies. On the other hand, the surface thermodynamic potential per unit area ,ω_s, decreases monotonically with x. The quantities σ_s and ω_s are the same for symmetric nuclear matter, since there is no neutron skin in this case.

The surface energy per unit area and the thermodynamic potential per unit area vary as δ_o^2 for small δ_o. The DM predicts

$$a_s = a_s(\delta_o=0) + (9J^2/4Q + 2a_{s0}L/K_o)\ \delta_o^2 = a_s(\delta_o=0) + S_{sE}\delta_o^2 \qquad (6.12)$$

$$\Omega_s = \Omega_s(\delta_o=0) - (9J^2/4Q - 2a_{s0}L/K_o)\ \delta_o^2 = \Omega_s(\delta_o=0) + S_{s\Omega}\delta_o^2 \qquad (6.13)$$

for a semi-infinite slab. We have extracted values of Q from our results (Fermi to a power and ETF+SO with $\eta_1 = 1/18$) for t, a_s and Ω_s using eqs. (6.11), (6.12) and (6.13). These are listed in table 1. The fact that the three values of Q for each interaction are very close (they should be strictly equal in an exact variational calculation) indicates that our restricted variational calculations provide a good approximation to exact variational results; in particular to the DM which for small asymmetries is an exact variational calculation. It is worth pointing out that similar results of Q from variation with a Fermi function ($p_i = 1$) show more scatter. We will return to a discussion of the surface symmetry coefficient S_s in sect. 6D. We note now, however, that S_s varies considerably between different forces.

C. CURVATURE PROPERTIES

We now present results for curvature properties. In fig. 8, we show the curvature energy per unit length, $\sigma_{c,R} = E_c/(8\pi R) = a_c/(8\pi r_o)$, and the curvature thermodynamic potential per unit length, $\omega_{c,R} = \Omega_c/(8\pi R)$, for several interactions. At $x = 0.5$, ω_c ranges from 0.28 to 0.47 MeV fm^{-1}, corresponding to $a_c = E_c/A^{1/3}$ ranging from 8.2 to 13.5 MeV. For all Skyrme forces the curvature energy grows quadratically with decreasing x close to x=0.5, reaches a maximum and then decreases much like the surface energy. The curvature thermodynamic potential per unit length decreases quadratically with decreasing x close to 0.5 and approaches zero as $x \to 0$. The quadratic dependence does not hold for as wide a range of δ_o as for the surface energy per unit area; it is however a good approximation in the range relevant for laboratory nuclei ($\delta_o^2 \leq 0.04$).

In analogy with the surface symmetry coefficient S_s, the curvature symmetry coefficient S_c is defined as:

$$a_c = a_c(\delta_o=0) + S_c\delta_o^2 \ . \qquad (6.14)$$

The results for the various interactions are listed in table 3. As in the case of the surface symmetry coefficient, there are large variations between forces in the curvature symmetry coefficient.

D. COMPARISONS WITH OTHER RESULTS

In comparing our results with results of Hartree-Fock calculations of finite nuclei, it is essential to use a smoothing procedure to obliterate the shell effects which are inherent in these calculations. The results of Dworzecka and Moszkowski[35] for finite nuclei ($A \approx 300$) demonstrate the uncertainties involved in simple smoothing procedures. Furthermore, curvature effects in such nuclei are not negligible.[15] Hence we compare our results only to those HF calculations done for semi-infinite slabs, or for very large nuclei ($A \geq 3000$) where contributions from shell structure and curvature are small.[27]

In tables 2 and 3, we list our results for several cases, along with other variational calculations (both exact and restricted) as well as those HF results which meet the above criteria. Results for three types of restricted variational (RV) calculations are shown. These are characterized by the form of the density profile used: RV1 denotes a Fermi function ($p_i = 1$), RV2 denotes a Fermi function to a power ($p_i \neq 1$), and RV3 denotes a Fermi function to a power multiplied by a Gaussian.[29] The RV3 calculations are for finite nuclei and include the Coulomb interaction; the Gaussian is included in order to allow for a depression in the central region of the density produced by the mutual repulsion between the protons. Each variational calculation is labeled by the kinetic energy functional used: TF, ETF, ETF+SO, or ETF4 (including $\hbar^4$ terms). ETF1 denotes calculations performed with $\eta_1 = 1/36$, ETF2 denotes those with $\eta_1 = 1/18$, and ETF3 denotes those with $\eta_1 = 0.08$. Table 2 contains results for symmetric matter properties, a^{90-10}, a_s, and a_c. Table 3 contains symmetry properties, t/δ_o, S_s, and S_c,

which are extracted from fits to our results for small δ_o. Note that there are two values of S_s and S_c; the top value is extracted from Ω_s or Ω_c, and the bottom one is obtained from a_s or a_c. In extracting S_s from a_s, we have applied the finite nucleus corrections discussed in sect. 6E, and hence the value listed is the appropriate one to use in mass formulae written in terms of the total asymmetry $I = (N-Z)/A$, not the bulk asymmetry $\delta_o = (\rho_{no}-\rho_{po})/\rho_o$.

From table 2, we see that the restricted variation RV1 underestimates the surface diffuseness a^{90-10} by 10-20% compared to HF and exact variations. Increasing the variational space by using a Fermi to a power distribution reduces this discrepancy, but does not eliminate it. The ETF corrections increase a^{90-10}, but SO terms reduce it again, as can be seen from the discussion in appendix C.

In general, for symmetric matter, the restricted variation results in lower values for the power p in eq. (4.2) for forces with larger incompressibilities. For the ETF2+SO case ($\eta_1 = 1/18$), p has the values 1.6, 2.4 and 4.1 for SI', SIII, and SkM*, respectively. In ref. 43, ETF4+SO corrections were included; the results for p for SIII and SkM* were found to be 1.34 and 1.78, respectively. Insofar as p controls the asymmetry of the optimum density profile around $z = z_{n,p}$, these differences point to the sensitivity of the surface behavior to the choice of $\tau(r)$.

The surface energy of symmetric matter is highest for the Fermi function case (RV1), intermediate for Fermi to a power (RV2), and lowest for the exact variation, as expected since the bulk energy is the same for all three cases. One would expect the RV3 case to have a lower value of a_s than the corresponding RV2 case; this, however, is not borne out. This may be due to the fact that the RV3 calculation[29] involves a mass formula fit to finite nuclei, which contains more uncertainties than a calculation of the semi-

infinite slab. As with a^{90-10}, the inclusion of the ETF corrections increases a_s, and the inclusion of SO terms lowers it. A comparison of ETF1+SO and ETF4+SO (which has $\eta_1 = 1/36$) shows that $\hbar^4$ corrections increase a_s. The HF results for a_s, when the SO correction of 1.5-2.0 MeV is subtracted from the results of refs. 27 and 39 (as explained in sect. 5), are in good agreement with the variational results, particularly the RV2, ETF2+SO (Fermi to a power, $\eta_1 = 1/18$) case.

The curvature energy of symmetric matter is increased by the ETF corrections and decreased by SO terms. Increasing the variational space increases a_c, in contrast to the behavior of a_s. It would be interesting to extract the curvature energy from HF calculations for comparison.

From table 3, we see that the neutron skin thickness is decreased by the inclusion of the ETF and SO terms, but increased by the ETF4 terms. It also increases from the restricted to HF or exact variations, in a similar manner as a^{90-10}.

The absolute value of the surface symmetry coefficient decreases when the ETF or SO terms are added, and increases with the inclusion of ETF4 terms. The curvature symmetry coefficient decreases in absolute value when SO terms are added. Otherwise, there seems to be no obvious trends in either S_s or S_c. As discussed in appendix B, large uncertainties are to be expected in these quantities, especially when extracted from mass formula fits. However, more constraints on the values of S_s may be imposed by considering the ratio $|S_s/J|$, which needs to be constrained in a description of the giant dipole resonance[37] and the difference between neutron and proton rms radii.[46]

E. CORRECTIONS FOR A FINITE NUCLEUS

In finite nuclei, the surface tension causes a compression of the interior. Consequently, the central density, ρ_o, is raised above the infinite matter saturation density, ρ_{NM}, by an amount $|\delta\rho_0|_{comp} = \rho_{NM}$ $(6a_{s0}/K_o)$ $A^{-1/3}$. On the other hand, inclusion of Coulomb energy decreases the central density by an amount $|\delta\rho_0|_{Coul} = \rho_{NM}$ (a_{Coul}/K_o) $Z^2A^{-4/3}$. Combining these two, we obtain, for small δ,

$$\rho_o = \rho_{NM} \left[1 - (3L/K_o)I^2 + |\delta\rho_0|_{comp} - |\delta\rho_0|_{Coul}\right] , \qquad (6.15)$$

where $I = (N-Z)/A$.

For the energy in eq. (1.1), the compressional effect leads to an additional term $E_{comp} = -a_{comp} A^{1/3}$, where $a_{comp} = 2a_{so}^2/K_o$. In the literature, this term is often referred to as a correction to the curvature energy, since it has an $A^{1/3}$ dependence. The values of a_{comp} are 1.62, 1.99, 2.78, and 2.98 MeV for SI', SIII, SkM, and SkM*, respectively.

We have obtained a positive value of S_s in connection with E_s, but a negative surface symmetry coefficient is used in mass formulae fits to nuclei. This is likely to cause some confusion regarding the sign of S_s. The following explanation is intended to clear this confusion.

Mass formulae are written in terms of the total asymmetry $I = (N-Z)/A$, and we have used the asymmetry $\delta_o = (\rho_{no}-\rho_{po})/\rho_o$ in the center of the nucleus. It can be shown in the droplet model[18] that the total (bulk + surface) symmetry energy can be written as

$$E_{sym} = J\delta_o^2 A + (9J^2/4Q + 2a_{s0}L/K_o)\ \delta_o^2\ A^{2/3} \qquad (6.16)$$

or

$$E_{sym} = J\, I^2\, A - (9J^2/4Q - 2a_{s0}L/K_o)\, I^2\, A^{2/3}\ , \qquad (6.17)$$

for large A and small δ_o^2 (or I^2).

This can be understood physically as a trade-off between bulk and surface symmetry energies. The bulk symmetry term $J\delta_o^2 A$ is written in terms of the correct bulk asymmetry δ_o. Since the asymmetry in the surface is larger than in the bulk (due to the neutron skin), the relative lack of protons in the surface causes the surface region to be less bound, and hence the surface symmetry energy is positive. In terms of I, however, the bulk term JI^2A overestimates the loss of bulk binding, since it overestimates the asymmetry. The surface term must make up for this by entering with the opposite sign, i.e., a system with uniform asymmetry I (and thus no neutron skin) can lower its energy by decreasing the asymmetry in the bulk region and putting the extra neutrons into a neutron skin.

7. APPLICATIONS

To illustrate the role played by surface and curvature energies, we discuss two applications in which their values for $x < 0.5$ (i.e., in the neutron rich regime) are explored. In the nuclear physics case, the properties of the liquid drop model (LDM) fission barrier for the nucleus ^{240}Pu ($x = 0.392$) are calculated. In the astrophysics case, features of the phase transition between nuclei and bubbles are examined in the region of $x \sim 0.3$.

A. FISSION BARRIER PROPERTIES

A sensitive test of the calculated surface and curvature energy constants is provided by the systematics of fission barrier heights and the shapes of the saddle point configurations. The measured spontaneous fission half-lives provide information about fission barrier heights, while the measured angular distributions of fission fragments may be related to the effective moment of inertia of the saddle point configuration.[40,41] Valid comparisons between data and theoretical calculations also involve considerations of nucleonic shell and pairing effects,[42] a task beyond the scope of this work. We therefore restrict ourselves to the calculation of the so-called LDM barriers with the aim of demonstrating the importance of including curvature effects.

For small δ_o or I = (N-Z)/A, the energy of a deformed nucleus may be represented approximately using a linearized version of the DM.[41] Even for heavy nuclei, such an approximation does not reproduce quantitatively the results of a restricted variational calculation performed for a finite nucleus.[43] However, for illustrating the role of curvature corrections, this approximation gives results that are in accordance with the more exact calculations of ref. 43.

Defining the deformation energy, E_{Def}, of a nucleus as the energy for some deformation minus the energy of the same but spherical nucleus, we have

$$E_{Def} = a_{s0}(1 + \kappa_s I^2)A^{2/3}(B_s - 1) + a_{c0}(1 + \kappa_c I^2)A^{1/3}(B_c - 1)$$

$$+ a_{Coul}Z^2A^{-1/3}(B_{Coul}-1) - a_{comp}A^{1/3}(B_{comp}-1) - a_{red}Z^2A^{1/3}(B_{red}-1). \quad (7.1)$$

In eq. (7.1), $\kappa_{s,c} = S_{s,c}/a_{s0,c0}$. For ETF2+SO with $\eta_1 = 1/18$, $\kappa_s = -2.1$,

-1.6, -2.9, and -2.8, and κ_c = 0.7, 1.6, 0.84, and 0.94 for the forces SI', SIII, SkM, and SkM*, respectively. The Coulomb energy constant is given by $a_{Coul} = 3e^2/(5r_{oC})$ + small corrections, where $r_{oC} = (3/4\pi\rho_0)^{1/3}$ fm. The last term in eq. (7.1) represents the contribution from the Coulomb redistribution energy. In terms of the DM coefficients, $a_{red} = (a^2_{Coul}/84)(4.5/K_o + 0.25/J)$. The quantities B_i which introduce shape dependence are given by the ratios of the deformed to spherical energies for each component.

For saddle shapes, E_{Def} gives the fission barrier height E_{Bar}. Defining the energy unit $E^0 = E^0_s + E^0_c + 2E^0_{comp}$ (the superscript 0 refers to the spherical shape) and dimensionless parameters $d_\xi = (E^0_{Coul}/2 - E^0_{red})/E^0$, $d_\eta = -E^0_c/E^0$, $d_\varsigma = -E^0_{red}/E^0$ and $d_\chi = -E^0_{comp}/E^0$, one may obtain a formula for the relative barrier $B_{Bar} = E_{Bar}/E^0$ that does not depend explicitly on the mass and neutron numbers:

$$B_{bar} = (B_s - 1) + 2d_\xi(B_{Coul} - 1) + d_\eta(B_s - B_c) - d_\varsigma(2B_{Coul} + B_{red} - 3)$$

$$+ d_\chi(2B_s - B_{comp} - 1) \quad . \tag{7.2}$$

In our calculations, we have used the shape parametrization of ref. 42. Two parameters c and h describe the axially symmetric shapes: the nuclear elongation is given by c and the neck thickness by h. The shape dependences of B_i were calculated using the relations in appendix A III.e of ref. 41. Saddle point shapes were found by searching for maxima in $E_{Def}(c,\tilde{h})$ versus c, where $\tilde{h}$ was obtained by the minimization relationship: $\partial E_{Def}(c,h)/\partial h|_{\tilde{h}} = 0$.

The influence of curvature, compression, and Coulomb redistribution may be studied independently of the other by varying only one of the parameters d_η, d_ς or d_χ in eq. (7.2). The effect of the compression energy is to

decrease B_{bar} by a very small amount. The influence of the Coulomb redistribution energy is greater than that of compression, and it tends to increase B_{Bar} but only by a small amount. The curvature energy has the largest effect of increasing B_{Bar}.

To focus on the role of curvature, we have performed calculations with and without the inclusion of the curvature contribution to E_{Def}, for ^{240}Pu, using constants deduced for the ETF2+SO case ($\eta_1 = 1/18$). For comparison, we treat the LDM barrier properties calculated by Brack et al.[42] as a bench mark. In ref. 42, the main features of the LDM fission barrier, viz., (E_{Bar}, c_{sad}) were determined to be (3.8±0.5 MeV,1.45±0.05) from an analysis of both the LDM contribution and the shell corrections to the deformation energy. Without the inclusion of curvature energies, we were unable to obtain a barrier for the forces SI', SkM and SkM*, since the Coulomb energies dominated the surface energies for all elongations, $c > 1.1$. However, for the SIII force we found $(E_{Bar}, c_{sad}) = (2.7\ MeV, 1.47)$; this is mainly due to the fact that the surface energy for the SIII force is larger in magnitude than for the other forces. With the inclusion of curvature energies, our results for (E_{Bar}, c_{sad}) for SI', SkM and SkM* were (2.4 MeV,1.47), (1.4 MeV,1.40) and (3.55 MeV, 1.59) respectively, while, for SIII we found E_{Def} in excess of 15 MeV. Of the forces considered, SkM* gives reasonable barrier properties, although c_{sad} is slightly larger than the empirical value. In ref. 43, this discrepancy is also removed by considering ETF4+SO corrections to $\tau(r)$. A discussion of the influence of curvature and compression energies on the slope of the potential energy surface from saddle to exit and scission may be found in ref. 47.

We note that in most empirical determinations of fission barrier properties, curvature corrections are included approximately by rescaling the

surface energy constant, a_s. This procedure entails equating the shape dependence of B_c to that of B_s. The shape dependence of B_c flattens the E_{Def} versus c curve near the top of the barrier. The errors are, however, small in that the the two procedures result in similar features of the barrier. Given the uncertainties in the surface and curvature symmetry coefficients, one may well choose a rescaled a_s in favor of including curvature corrections explicitly. From our fission calculations, however, we may conclude that the magnitude of a_c ($\sim$ 10 MeV) calculated from Skyrme forces such as SkM* gives acceptable barrier properties. With these numbers in hand, we may then explore physical situations in which the explicit inclusion of curvature properties has a marked effect. The next section is devoted to one such application.

B. THE NUCLEUS-BUBBLE PHASE TRANSITION IN DENSE MATTER

In zero temperature dense matter below about half the saturation density, nuclei are in equilibrium with a dilute neutron vapor or a vacuum depending on the proton fraction. There is an approximately uniform background of electrons (and possibly neutrinos, which we neglect) that may be treated independently of the baryons. At densities above half the saturation density, the nuclei merge into a uniform nucleon liquid. Lamb et al.[22] showed that an intermediate stage, in which the voids between the nuclei form bubbles, could occur. Later, Ravenhall, Pethick and Wilson[44] suggested that other intermediate configurations, which they termed 'spaghetti' and 'lasagna' (being the 2- and 1- dimensional analogues of 3-dimensional nuclei and bubbles), could occur as well. Because the energy differences between any two of these phases is small ($\leq$ 0.1 MeV/nucleon), the

positions of the various phase transitions are sensitive to the accuracy with which one constructs a nuclear model. In particular, the inclusion of curvature corrections to the nuclear surface energy is important.[7,33] Although the energy is modified at the 10% level, curvature corrections enter for bubbles with the opposite sign as for nuclei. The result is that the nucleus-bubbles transition is shifted by up to 40% toward lower densities.[48]

Here we present a simplified model of the nucleus-bubble phase transition. We assume that there is no dilute neutron vapor, and neglect the effects of compression of the dense phase (i.e., we assume it has the saturation density ρ_o). However, we will include the effects of the neutron skin of the dense phase. We will only consider 3-dimensional configurations here.

The energy per unit volume of the phase with nuclei is

$$W_N = u(W_b + W_{s,N} + W_{c,N} + W_{Coul,N}) + W_e \ , \tag{7.3}$$

and that of the bubbles is

$$W_B = (1-q)W_b + q(W_{s,B} + W_{c,B} + W_{Coul,B}) + W_e \ . \tag{7.4}$$

In eqs. (7.3) and (7.4), W_b is the bulk energy density of the dense phase, W_s is the surface energy, W_c is the curvature energy and W_{Coul} is the Coulomb energy, all divided by the nuclear or bubble volume. W_e is the electron energy density. The fraction of space filled by the dense phase is denoted by u, and q is the fraction of space filled by the dilute phase. Thus u = 1-q. If the dense phase is assumed to have density ρ_o, then $u = \rho/\rho_o$. The phase transition will be first order, occuring in density near where $W_N = W_B$. Its extent is determined by a Maxwell construction.

The surface energy densities $W_{s,N}$ and $\bar{W}_{s,B}$ are

$$W_{s,N} = 3\sigma_{s,p}/R_{p,N} = 3(\omega_s + \mu_n(R_{n,N}-R_{p,N})\rho_{no})/R_{p,N} \tag{7.5}$$

and

$$W_{s,B} = 3\sigma_{s,p}/R_{p,B} \ , \tag{7.6}$$

where $R_{p,N}$ and $R_{p,B}$ are the nuclear and bubbular proton radii, $\sigma_{s,p}$ is the surface energy per unit area taken with respect to the proton radius, ω_s is the surface thermodynamic potential per unit area, or surface tension, and μ_n is the neutron chemical potential. We have chosen the proton radius R_p as our surface, since this choice simplifies the Coulomb energy calculation.

The curvature energy densities are

$$W_{c,N} = 6\sigma_{c,p}/R^2_{p,N} = 6(\omega_{c,p} + \tfrac{1}{2}(R_{n,N}-R_{p,N})^2\rho_{no}\mu_n)/R^2_{p,N} \tag{7.7}$$

and

$$W_{c,B} = -6\sigma_{c,p}/R^2_{p,B} \ , \tag{7.8}$$

where $2\sigma_{c,p}/R_p$ is the curvature energy per unit area and $2\omega_{c,p}/R_p$ is the curvature thermodynamic potential per unit area, all taken with respect to the proton radius.

The Coulomb energy densities are

$$W_{Coul,N} = (4/5)\pi e^2 x^2 \rho_o^2 R^2_{p,N} f(u) \tag{7.9}$$

and

$$W_{Coul,B} = (4/5)\pi e^2 x^2 \rho_o^2 R_{p,B}^2 f(1-u) \ , \qquad (7.10)$$

where $x = Z/A$ is the proton (electron) fraction of the matter, and $f(u) = 1 - 1.5u^{1/3} + 0.5u$. The derivation of these energies is described in detail in reference 22.

The optimum sizes for the nuclei (bubbles) are determined by minimization of W_N (W_B) with respect to $R_{p,N}$ ($R_{p,B}$) at each density. The quantity u and, as discussed in ref. 22, the ratio of the number of surface neutrons $N_s = (\rho_{no}-\rho_{nd})(4\pi/3)(R_n^3-R_p^3)$, to the nucleon number A, are fixed in this minimization. Therefore only the thermodynamic potentials survive:

$$3\omega_s/R_{p,N} + 12\omega_{c,p}/R_{p,N}^2 = 2W_{Coul,N} \qquad (7.11)$$

and

$$3\omega_s/R_{p,B} - 12\omega_{cp}/R_{p,B}^2 = 2W_{Coul,B} \ . \qquad (7.12)$$

In the absence of curvature, $W_N = W_B$ when $u = q = 1/2$, or when $\rho = \rho_o/2$. This result is independent of the magnitude of $\sigma_{s,p}$. With curvature, it is straightforward to show that $W_N = W_B$ when $u = 1/2 + \Delta$, where Δ is approximately given by

$$\Delta \approx -\alpha(\omega_{c,p}/\omega_s)R_o^{-1}(2 - 2\sigma_{s,p}/\omega_s + 3\sigma_{c,p}/\omega_{c,p})/(1 + 2\sigma_{s,p}/\omega_s) \ , \qquad (7.13)$$

with

$$R_o = [15\omega_s/\{8\pi e^2 x^2 \rho_o^2 f(0.5)\}]^{1/3} \qquad (7.14)$$

and

$$\alpha = 4f/(6f + df/du)|_{u=0.5} \approx 3.775 \ . \qquad (7.15)$$

Note that in the case x=0.5 when there is no neutron skin and $\omega_s = \sigma_s$ and $\omega_c = \sigma_c$, the ratio of the final two terms in eq. (7.13) is unity.

Our results for Δ for the different Skyrme forces are listed in table 4, for three different values of x. An important result is that the nucleus-bubble phase transition occurs for all the interactions studied. In general, curvature effects are large and become more important with decreasing proton fraction of the matter. In the case x = 0.3, the inclusion of curvature may shift the transition to 40% lower densities. For very low proton fractions, Δ becomes positive. This can be easily seen by expanding eq. (7.13) in R_n-R_p (which is the same for nuclei and bubbles). To first order, we can set $\sigma_{c,p} \approx \omega_{c,p}$ and $\sigma_{s,p} = \omega_s + (R_n-R_p)\rho_{no}\mu_n$. Upon expansion, the final two terms in eq. (7.13) become $1 - (4\rho_{no}\mu_n/3\omega_s)(R_n-R_p)$. At $x \approx 0.34$, μ_n becomes positive, while R_n-R_p and ρ_{no}/ω_s increase monotonically with decreasing x. Thus, for sufficiently small x, Δ becomes positive and the nucleus-bubble transition is shifted to higher densities. In fact, as x is decreased further, the nuclei will disappear directly via a transition to uniform matter (near $u \approx 0.8$) rather than passing through an intermediate bubbular phase.[7,33] As indicated in table 4, the bubble phase already does not appear in the case x = 0.1 for the SkM and SkM* interactions.

A Maxwell construction may be performed to find the width of the transition which is roughly centered around the density determined above, ρ_t

= $(1/2 + \Delta)\rho_o$. The phase transition extends between the densities ρ_N and ρ_B, whose values are given in table 4 for both TF and ETF+SO ($\eta_1 = 1/18$, $\eta_2 = 1/3$) formalisms with the interactions SI', SIII and SkM. The transition is observed to become quite wide for small values of x, especially for SIII.

8. CONCLUSIONS

We have used a restricted variational approach with Skyrme-type effective forces to calculate surface and curvature properties of neutron-rich matter. When the density profile is taken to be a Fermi distribution to a power, excellent agreement with exact variational results is found. The surface thickness in the restricted variational method tends to be too low in general. There are large variations among the results for different interactions, especially in the surface symmetry energy, curvature energy and curvature symmetry energy. This suggests that experimental information not directly related to the total energy of the nucleus should be used to fix the parameters of a given interaction. The parameters of the SkM and SkM* forces were constrained to provide a consistent description of isovector properties of nuclei, such as the giant dipole resonances. As a result, they also describe the differences between neutron and proton root mean square radii reasonably well. For this reason, one can argue in favor of the predicted asymmetry dependences from these forces.

For proton fractions corresponding to laboratory nuclei, the droplet model (DM) gives an adequate representation of the asymmetry dependence of the energies as well as other surface and curvature properties. To facilitate the exploration of the DM with Skyrme type effective forces we have related the parameters of the DM to those of Skyrme forces. Our results

for fission barriers clearly demonstrate the importance of including curvature energies.

In astrophysical applications, surface and curvature energies for smaller proton fractions are required. Our investigation of the nucleus-bubble phase transition shows that the density at which the transition occurs is sensitive to the variations in surface and especially curvature energies among the different interactions. Since differences in curvature energies arise mainly from differences in the incompressibility, it is probably best to rely on those forces which reproduce the empirical value for the incompressibility and join smoothly with neutron matter calculations.

In this work we have dealt with surface and curvature properties for the zero temperature case. A possible direct extension would be to consider the finite temperature case. Similar studies with finite range nucleon-nucleon forces would also be interesting. Quantitative calculations in this regard together with experimental constraints on the asymmetry dependence of effective forces may enable us to unambiguously determine the surface and curvature symmetry energies in simplified equations of state for dense matter.

Authors K. K. and J. T. wish to thank Bill Myers and Wladek Swiatecki for many helpful discussions.

Supported in part by the U.S. Department of Energy under contract DE-AC03 76SF00098 with Lawrence Berkeley Laboratory and in part by the U.S. Department of Energy under contract DE-AC02-76ER13001 with the State University of New York at Stony Brook.

APPENDIX A

RELATIVE CONTRIBUTIONS TO THE CURVATURE ENERGY

In general, the curvature energy contains two contributions (see eq. 3.11). The second term, involving a derivative with respect to $k = 2/R$, is nonvanishing only when there are terms in the energy density ϵ which are of the form $f(\rho_i,\rho_j)\nabla^2\rho_i$. Using $\nabla^2\rho_i = \partial^2\rho_i/\partial r^2 + \frac{2}{r}\,\partial\rho_i/\partial r$ and integrating by parts, we have

$$\int_{-\infty}^{\infty} f(\rho_i,\rho_j)\nabla^2\rho_i\,dz\big|_{k=0} = -\int_{-\infty}^{\infty} (\nabla\rho_i)(\nabla f)\,dz\big|_{k=0}\ , \tag{A.1}$$

and

$$\int_{-\infty}^{\infty}(z-R)f(\rho_i,\rho_j)\nabla^2\rho_i\,dz\big|_{k=0} + \int_{-\infty}^{\infty}[\partial\{f(\rho_i,\rho_j)\nabla^2\rho_i\}/\partial k]_{k=0}dz$$

$$= -\int_{-\infty}^{\infty} (z-R)(\nabla\rho_i)(\nabla f)\,dz\big|_{k=0}\ . \tag{A.2}$$

Therefore, if we replace any term in ϵ of the form $f(\rho_i,\rho_j)\nabla^2\rho_i$ by $-[(\nabla\rho_i)^2\partial f/\partial\rho_i + (\nabla\rho_i)(\nabla\rho_j)\partial f/\partial\rho_j]$, the surface and curvature energies are unchanged, although the relative contributions of the two terms in eq. (3.11) are changed. Hence, it is inappropriate to attach any physical significance to the two terms individually; only the sum is physically meaningful.

APPENDIX B

THE SURFACE SYMMETRY COEFFICIENT

We find that there are larger variations in the surface symmetry coefficient S_s from interaction to interaction than in the surface energy of symmetric matter a_s or the bulk symmetry coefficient S_V. Qualitatively, we can understand this as follows: Let us consider the example of a finite nucleus with total asymmetry $I = (N-Z)/A$, and write two possible mass formula fits to the total energy per particle:

$$E_{tot}/A = -16 + S_V I^2 + a_s A^{-1/3} - S_s I^2 A^{-1/3} \qquad (B.1)$$

$$E'_{tot}/A = -16 + S_V' I^2 + a_s' A^{-1/3} - S_s' I^2 A^{-1/3} \ , \qquad (B.2)$$

with different values of a_s, S_V, and S_s. We neglect, for simplicity, the curvature and Coulomb energies. We denote by the quantity $\Delta = (E_{tot}-E_{tot}')/A$ the acceptable uncertainty in the fits to the total energy per particle. Equating the two total energies in eqs. (B.1) and (B.2) to within the term Δ, we obtain

$$S_s - S_s' = (S_V - S_V')A^{1/3} + (a_s - a_s')/\delta_o^2 + \Delta A^{1/3}/\delta_o^2 \ . \qquad (B.3)$$

We note that (S_V-S_V') and (a_s-a_s'), both of which can vary by a few MeV between interactions, are both multiplied by large numbers (when δ_o is small). Furthermore, the magnitude of the term containing Δ is also in general large. This leads to a value of (S_s-S_s') which is much greater than

either (S_V-S_V') or (a_s-a_s'). Thus, to determine a reliable value for S_s, experimental information not directly related to the total energy of the nucleus should be used to fix the parameters of a given interaction.

APPENDIX C

DEPENDENCE OF SURFACE AND CURVATURE PROPERTIES ON NUCLEAR FORCE PARAMETERS

To focus on the dependence of the surface and curvature properties on the nuclear force parameters and the inclusion of extended Thomas-Fermi (ETF) terms we consider the following simple model. We treat, for simplicity, only the case of symmetric matter. We first approximate the energy density ϵ by a parabolic relation:

$$\epsilon = \epsilon_o \rho/\rho_o + k\rho(1 - \rho/\rho_o)^2 + q(\rho)(\nabla\rho)^2 \ . \qquad (C.1)$$

The constant k can have at least two interpretations. For interactions with relatively large incompressibilities, like SI' and SIII, one should use $k = K_o/18$, which makes eq. (C.1) a fit to nuclear matter near ρ_o. But for interactions with moderate to low incompressibilities, like SkM, this value of k leads to an energy per particle that remains large even at low densities. If we desire the energy per particle ϵ/ρ to vanish as $\rho \to 0$, then $k = |\epsilon_o/\rho_o| \approx 16$ MeV might be used. We will consider both cases in what follows.

In eq. (C.1), $q(\rho)$ contains the gradient corrections to the energy. In the Thomas-Fermi (TF) approximation, q is constant and equals

$$q^{TF} = A^{TF} = (9t_1 - 5t_2)/64 \qquad (C.2)$$

in terms of Skyrme parameters. In the ETF formalism, with the spin-orbit interactions included, we may write

$$q(\rho) = A^{ETF} f(\rho/\rho_o) \ , \tag{C.3}$$

where, to lowest order in $x = \rho/\rho_o$,

$$f \approx 1 + B/x + Cx \ . \tag{C.4}$$

From eq. (C.1), we can find A^{ETF}, B and C in terms of Skyrme parameters:

$$A^{ETF} = A^{TF} + (3t_1 + 5t_2)(\eta_1 - \eta_2)/16 \ , \tag{C.5}$$

$$B = (\hbar^2/2m)\eta_1/(\rho_o A^{ETF}) \ , \quad C = -(9/32)W_o^{\,2}(2m\rho_o/A^{ETF}\hbar^2) \ . \tag{C.6}$$

The Euler-Lagrange equation for the density profile of a slab, eq. (4.1), becomes

$$q(\rho)(\nabla\rho)^2 = k\rho(1-\rho/\rho_o)^2 \ . \tag{C.7}$$

We define a dimensionless distance function w by

$$w(x) = (k/A\rho_o)^{1/2} z(x) = \int_x^1 (f/x)^{1/2}(1-x)^{-1}\, dx \ , \tag{C.8}$$

where the last equality follows from eq. (C.7). Using eq. (3.12), we find that the equivalent matter radius $R = \int_0^1 w\, dx$. The 90% - 10% surface thickness can be found from eq. (6.9):

$$a = (A/k\rho_o)^{1/2}[w(0.1) - w(0.9)] \ . \qquad (C.9)$$

The surface energy per unit area is

$$\sigma_s = \int_{-\infty}^{\infty} k\rho(1-\rho/\rho_o)^2 \, dz = 2(Ak\rho_o^3)^{1/2} \int_0^1 (fx)^{1/2}(1-x) \, dx \ . \qquad (C.10)$$

The curvature energy per unit length is

$$\sigma_c = \int_{-\infty}^{\infty} k\rho(1-\rho/\rho_o)^2(z-R) \, dz$$

$$= 2A\rho_o^2[\int_0^1(fx)^{1/2}(1-x)w \, dx - \int_0^1 w \, dx \int_0^1(fx)^{1/2}(1-x) \, dx]. \qquad (C.11)$$

Note that w is defined relative to an arbitrary zero point, which, however, cancels in the expressions for σ_c and a.

In the TF case, all the integrals can be performed analytically. We find

$$w^{TF} = \ln[(1 - x^{1/2})/(1 + x^{1/2})] \quad , \ a^{TF} = 2.982 \ (A^{TF}\rho_o/k)^{1/2} \ ,$$

$$\sigma_s^{TF} = (8/15)(A^{TF}k\rho_o^3)^{1/2}, \quad \sigma_c^{TF} = (7 - 8\ln 2)2A^{TF}\rho_o^2/15 \ . \qquad (C.12)$$

These results give the approximate dependence of the surface and curvature energies on the effective incompressibility k, the gradient term A^{TF}, and the saturation density ρ_o. If one takes the point of view that ρ_o is known to be fixed near 0.16 fm^{-3}, then, for a given surface tension (which is fairly well established through the semi-empirical mass formula), the quantities A^{TF} and k are inversely proportional. Hence both the surface thickness and the curvature tension can be viewed as being proportional to either A^{TF} or k^{-1}.

Inverting the first equation of (C.12), we find that $x = \tanh^2(-w^{TF}/2)$. Hence, the density vanishes for $w^{TF} > 0$. For a more realistic description of the surface region, such as that given by a Hartree-Fock calculation, corrections to the TF approximation are needed.

In the ETF case, to within a few percent, we may approximate the results by the following expansions:

$$a^{ETF}/a^{TF} \approx (A^{ETF}/A^{TF})^{1/2} \ (1 + 1.1B + 0.3C)$$

$$\sigma_s{}^{ETF}/\sigma_s{}^{TF} \approx (A^{ETF}/A^{TF})^{1/2} \ (1 + 1.7B + .23C)$$

$$\sigma_c{}^{ETF}/\sigma_c{}^{TF} \approx (A^{ETF}/A^{TF}) \ (1 + 5.5B + 0.4C) \ . \qquad (C.13)$$

We observe that the spin-orbit corrections (the C terms) are opposite in sign to that of the η_1 terms for σ_s, σ_c and a, but their coefficients in eq. (C.13) are generally several times smaller. As a result, η_1 is the most important ETF parameter. The surface and curvature tensions both vary nearly linearly with its value. The density profile in the ETF case varies as $\exp(-z/\alpha)$, for $z \to \infty$, where $\alpha = \sqrt{(\hbar^2\eta_1/2mk)}$. Taking $k \approx 16$MeV and $\eta_1 \approx 1/18$ (0.08) we get $\alpha \approx 0.27$ (0.32) fm, showing the sensitivity of the slope of the surface profile at large distances to the value of η_1.

For the interactions SI', SIII, SkM and SkM*, results from eq. (C.13) are given in table 5. While a^{ETF}/a^{TF} is less than unity, and $\sigma_s{}^{ETF}/\sigma_s{}^{TF}$ is 0.99 - 1.1, the curvature energy can be increased by up to 60% by including extended Thomas-Fermi corrections. All results listed are for $k = K_o/18$, but values for $k = |\epsilon_o/\rho_o|$ may be derived from the quantity $\kappa = |18\epsilon_o/(\rho_o K_o)|$, which is also given, and the relations (C.8). Agreement with the detailed

numerical results in table 2 is good for SI' and SIII, and the surface energies of SkM and SkM* are reasonably represented by using $k = |\epsilon_o/\rho_o|$. For example, for the force SkM, the surface energy should be multiplied by $\kappa^{1/2}$, which gives 1.083 and 1.066 MeV fm^{-2} for TF and ETF, respectively. However, the surface thicknesses a are better fit by using the original value of k, and the curvature energy, which does not depend on k, is always too small by 0.04 - 0.06 MeV fm^{-1} for the latter two interactions. It can be concluded that interactions with large incompressibilities are better fit by the techniques presented in this appendix.

REFERENCES

1. G. Baym, H. A. Bethe, and C. J. Pethick, Nucl. Phys. **A175** (1971) 225
2. H. A. Bethe, G. E. Brown, J. H. Applegate, and J. M. Lattimer, Nucl. Phys. **A324** (1979) 487
3. J. M. Lattimer, Ann. Rev. Nucl. Part. Sci. **31** (1981) 337
4. H. A. Bethe, G. E. Brown, J. Cooperstein, and J. R. Wilson, Nucl. Phys. **A403** (1983) 625
5. G. Fuller, Astrophys. J. **252** (1982) 741;
   J. Cooperstein and J. Wambach, Nucl. Phys. **A420** (1984) 591
6. M. Barranco and J. Treiner, Nucl. Phys. **A351** (1981) 269;
   M. Prakash, J. Wambach, and Z. Y. Ma, Phys. Lett. **128B** (1983) 141
7. C. J. Pethick, D. G. Ravenhall, and J. M. Lattimer, Phys. Lett. **128B** (1983) 137
8. G. Bertsch and P. J. Siemens, Phys. Lett. **126B** (1983) 9
9. K. Kolehmainen, Ph.D. thesis, SUNY at Stony Brook (1983)
10. J. M. Lattimer and D. G. Ravenhall, Astrophys. J. **223** (1978) 314
11. P. Hohenberg and W. Kohn, Phys. Rev. **136** (1964) B864;
    J. Brueckner, R. Buchler, R. Clark, and R. Lombard, Phys. Rev. **181** (1969) 1543;
    R. Lombard, Ann. of Phys. **77** (1973) 380
12. T. H. R. Skyrme, Phil. Mag. **1** (1956) 1043;
    T. H. R. Skyrme, Nucl. Phys. **9** (1959) 615
13. S. A. Moszkowski, Phys. Rev. **C2** (1970) 402
14. J. P. Blaizot and B. Grammaticos, Nucl. Phys. **A355** (1981) 115
15. C. Guet, H. B. Håkansson and M. Brack, Proc. Workshop on Semiclassical Methods in Nuclear Physics, Grenoble (1981)

16. C. D. Bennett and D. G. Ravenhall, Phys. Rev. **C10** (1974) 2058

17. B. Grammaticos, Z. Physik **A312** (1983) 99

18. W. D. Myers and W. J. Swiatecki, Ann. of Phys. **55** (1969) 395;
W. D. Myers, Droplet Model of Atomic Nuclei (Plenum, New York 1977)

19. D. Vautherin and D. M. Brink, Phys. Rev. **C5** (1972) 626

20. H. von Groote, Proc. 3rd International Conference on Nuclei Far from Stability, Cargese, Corsica (1976)

21. W. D. Myers, W. J. Swiatecki, and C. S. Wang, Lawrence Berkeley Laboratory Report 16947

22. D. Q. Lamb, J. M. Lattimer, C. J. Pethick, and D. G. Ravenhall, Phys. Rev. Lett. **41** (1978) 1623;
J. M. Lattimer, C. J. Pethick, D. G. Ravenhall and D. Q. Lamb, Nucl. Phys. **A** (1984) in press.

23. B. Grammaticos and A. Voros, Ann. of Phys. **123** (1979) 359;
B. Grammaticos and A, Voros, Ann. of Phys. **129** (1980) 153

24. N. L. Balazs, Phys. Rev. **134** (1964) A841

25. N. L. Balazs and G. G. Zipfel, Jr., Ann. of Phys. **77** (1973) 139;
R. Baltin, Z. Naturforsch. **27a** (1972) 1176

26. D. Kessler and J. W. Negele, Phys. Rev. **C13** (1976) 1698

27. X. Campi and S. Stringari, Nucl. Phys. **A337** (1980) 313

28. C. F. Weizsacker, Z. Physik **96** (1935) 431

29. Y. H. Chu, B. K. Jennings, and M. Brack, Phys. Lett. **68B** (1977) 407

30. J. Treiner and H. Krivine, Orsay Preprint IPNO/TH 82-18.

31. M. Farine, J. Cote, and J. M. Pearson, Phys. Rev. **C24** (1981) 303

32. P. J. Siemens and V. R. Pandharipande, Nucl. Phys. **A173** (1971) 561

33. D. G. Ravenhall, C. J. Pethick, and J. M. Lattimer, Nucl. Phys. **A**, in press

34. H. Krivine and J. Treiner, Phys. Lett. **124B** (1983) 127

35. M. Dworzecka and S. Moszkowski, Phys. Rev. **C12** (1975) 619

36. M. Beiner, H. Flocard, N. V. Giai, and P. Quentin, Nucl. Phys. **A238** (1975) 29

37. H. Krivine, J. Treiner, and O. Bohigas, Nucl. Phys. **A336** (1980) 155

38. J. Bartel, P. Quentin, M. Brack, C. Guet, and H. B. Håkansson, Nucl. Phys. **A386** (1982) 79

39. D. G. Ravenhall, C. D. Bennett, and C. J. Pethick, Phys. Rev. Lett. **28** (1972) 978

40. A. Bohr and B. R. Mottelson, Nuclear Structure, vols. I and II (Benjamin, 1975)

41. R. W. Hasse, Ann. of Phys. **68** (1971) 317

42. M. Brack, J. Damgaard, H. C. Pauli, A. S. Jensen, V. M. Strutinsky, and C. Y. Wong, Rev. Mod. Phys. **44** (1972) 320

43. M. Brack, C. Guet and H. B. Håkansson, Phys. Rep. (submitted)

44. D. G. Ravenhall, C. J. Pethick, and J. R. Wilson, Phys. Rev. Lett. **50** (1983) 2066

45. B. Friedman and V. R. Pandharipande, Nucl. Phys. **A361** (1981) 502

46. S. Stringari and E. Lipparani, Phys. Lett. **117B** (1982) 141;
E. Lipparani and S. Stringari, Phys. Lett. **112B** (1982) 421.

47. J. Treiner, R. W. Hasse, and P. Schuck, J. Phys. Lett. **44** (1983) L-733.

48. P. Bonche and D. Vautherin, Astron. Astrophys. **112** (1982) 168;
S. Marcos, M. Barranco and J. R. Buchler, Nucl. Phys **A381** (1982) 507.

FIGURE CAPTIONS

Fig. 1. Asymptotic densities, ρ_o and ρ_d, in the nuclear and drip regions respectively, as functions of δ_o^2. The asymmetry parameter δ_o is given by $\delta_o=(\rho_{no}-\rho_{po})/\rho_o = (1-2x)$, where $x = \rho_{po}/\rho_o \sim Z/A$.

Fig. 2. The bulk incompressibility in the nuclear region as a function of $\delta_o^2 = (1-2x)^2$ for the interactions SI', SIII, and SkM*.

Fig. 3. Results of restricted variation (RV2, ETF+SO with $\eta_1 = 1/18$) for the diffuseness parameters a_n and a_p in as functions of the bulk asymmetry $\delta_o = (1-2x)$.

Fig. 4. Results of restricted variation for the powers p_n and p_n as functions of the bulk asymmetry $\delta_o = (1-2x)$ for the Skyrme interactions shown. For each interaction the larger value for the power is associated with the proton profile.

Fig. 5. The 90-10 surface thicknesses for the neutron and proton profiles as functions of the bulk asymmetry $\delta_o = (1-2x)$.

Fig. 6. Results of restricted variation for the neuton skin thickness, $t = z_n - z_p$, as a function of the bulk asymmetry $\delta_o = (1-2x)$ for the Skyrme interactions shown.

Fig. 7. The surface energy per unit area, $\sigma_{s,R} = E_{s,R}/(4\pi R^2)$, and the surface thermodynamic potential per unit area, $\omega_s = \Omega_s/(4\pi R^2)$, as functions of $\delta_o^2 = (1-2x)^2$. The upper set of curves give σ_s and the lower set give ω_s for the Skyrme interactions shown.

Fig. 8. The curvature energy per unit length, $\sigma_{c,R} = E_{c,R}/(8\pi R)$, and the curvature thermodynamic potential per unit length, $\omega_{c,R} = \Omega_{c,R}/(8\pi R)$, as functions of $\delta_o^2 = (1-2x)^2$. The upper set of curves give σ_c and the lower set give ω_c for the Skyrme interactions shown.

TABLE CAPTIONS

Table 1. The constants t_0 to t_3, x_0, x_3, γ and W_0 are parameters of the Skyrme forces listed. The constants J, K_o, L, M, and K_{sym} are the parameters of the droplet model deduced from their relations to the parameters of the Skyrme interaction. The DM parameter Q is obtained from fits to the surface symmetry coefficient for three values of the ETF coefficient η_1 (see text). The constants ρ_{NM} and r_o are obtained by solving for bulk equilibrium of symmetric nuclear matter.

Table 2. Comparison of results for the surface diffuseness parameter, a, the surface energy constant, a_s, and the curvature energy constant, a_c, for symmetric nuclear matter obtained from different approximations (denoted by ETF1, ETF2, ETF3, and ETF4) to the kinetic energy density. The legends RV1, RV2, and RV3 refer to restricted variational calculations with different forms for the density profile (see text). The legend PW refers to present work. Results from exact variational and Hartree-Fock calculations are also shown. HF results from refs. 27 and 39 do not include spin-orbit corrections; therefore a_s should be reduced by about 1.6 MeV before comparison with results containing SO corrections.

Table 3. Comparison of results for the ratio of neutron skin thickness to the bulk asymmetry parameter, t/δ_o, the surface symmetry coefficient, S_s, and the curvature symmetry coefficent, S_c, for small asymmetries δ_o obtained from different approximations to the kinetic energy density functional, $\tau(r)$. The various legends are explained in the caption for table 2. The two values for S_s and S_c are explained in the text.

Table 4. Results for the nucleus-bubble phase transition. The nucleus-bubble transition extends between ρ_N and ρ_B, as determined from a Maxwell construction. The percentage shift of the transition from $\rho_t = \rho_o/2$ due to the inclusion of curvature effects is 2Δ. All ETF calculations assume $\eta_1 = 1/18$ and include spin-orbit corrections.

Table 5. Comparison of approximate surface properties with exact results. All results are for x = 0.5. The first row for each interaction contains approximate results as per appendix C. The second row contains the numerical results from this paper. All ETF calculations assume $\eta_1 = 1/18$ and include spin-orbit corrections.

Table 1

Force	SI'	SIII	SkM	SkM*
Reference	3	36	37	38
t_o(MeV-fm^3)	-1057.3	-1128.75	-2645.0	-2645.0
t_1(MeV-fm^5)	235.9	395.0	385.0	410.0
t_2(MeV-fm^5)	-100.0	-95.0	-120.0	- 135.0
t_3(MeV-fm$^{3+3\gamma}$)	14463.5	14000.0	15595.0	15595.0
x_o	0.2885	0.45	0.09	0.09
x_3	0.2257	1.0	0	0
γ	1.0	1.0	1/6	1/6
W_o(MeV-fm^5)	120.0	120.0	130.0	130.0
J(MeV)	29.35	28.16	30.75	30.03
K(MeV)	370.3	355.3	216.6	216.6
L(MeV)	35.34	9.91	49.34	45.78
M(MeV)	1.400	1.667	1.822	1.875
K_{sym}(MeV)	-259.1	-393.7	-148.8	-155.9
Q(MeV)				
η_1 = 1/36	54	61	39	38
= 1/18	48	54	35	34
= 0.08	44	50	33	32
ρ_{NM}(fm^{-3})	0.1553	0.1453	0.1603	0.1603
r_o(fm)	1.154	1.180	1.142	1.142

Table 2

		a^{90-10} (fm)				a_s (MeV)				a_c (MeV)			
Method	Ref	SI'	SIII	SkM	SkM*	SI'	SIII	SkM	SkM*	SI'	SIII	SkM	SkM*
Restricted variation with a Fermi function (RV1)													
TF	PW	1.46	1.78	2.13	2.21	16.55	19.15	18.37	19.03	4.42	6.14	8.65	9.28
ETF1	PW	1.59	1.76	2.14	2.21	17.94	18.89	18.39	19.06	6.49	7.22	9.99	10.63
ETF1+SO	PW	1.33	1.57	1.85	1.94	15.03	16.94	15.94	16.70	5.75	6.61	8.72	9.36
ETF2	PW	1.77	1.93	2.32	2.40	19.97	20.82	20.02	20.63	9.03	9.75	12.92	13.56
ETF2+SO	PW	1.54	1.77	2.07	2.15	17.40	19.07	17.79	18.48	8.28	9.13	11.64	12.28
ETF3	PW	1.91	2.08	2.48	2.55	21.59	22.37	21.34	21.92	11.26	11.96	15.49	16.13
ETF3+SO	PW	1.70	1.93	2.24	2.31	19.25	20.75	19.27	19.91	10.52	11.35	14.22	14.85
ETF4+SO	15	-	-	-	-	-	18.30	17.18	-	-	4.87	6.09	-
ETF4+SO	43	-	-	-	-	-	18.13	16.85	17.51	-	-	-	-
Restricted variation with a Fermi function to a power (RV2)													
ETF1+SO	PW	1.44	1.75	2.15	2.26	14.87	16.55	15.37	16.05	6.28	7.50	9.96	10.74
ETF2+SO	PW	1.63	1.93	2.35	2.45	17.31	18.79	17.34	17.96	8.82	10.10	13.08	13.87
ETF3+SO	PW	1.78	2.08	2.51	2.61	19.18	20.54	18.89	19.46	11.06	12.38	15.80	16.60
ETF4+SO	43	-	1.95	2.31	2.39	-	18.04	16.60	17.22	-	9.52	12.19	12.82
Restricted variation with Fermi function to a power X Gaussian (RV3)													
ETF1+SO	29	-	-	-	-	-	18.64	-	-	-	10.6	-	-
Exact variation													
TF	33	-	-	-	-	15.4	-	-	-	-	-	-	-
TF	16	-	-	-	-	-	-	-	-	5.24	-	-	-
TF	14	-	2.14	-	-	-	17.84	-	-	-	-	-	-
ETF1	14	-	2.04	-	-	-	18.20	-	-	-	-	-	-
ETF1+SO	14	-	1.81	-	-	-	16.55	-	-	-	-	-	-
ETF1	17	-	-	-	-	-	-	-	-	-	10.8	-	-
Hartree-Fock													
no SO	27	-	2.20	2.64	-	-	20.4	18.6	-	-	-	-	-
no SO	39	-	-	-	-	19.2	-	-	-	-	-	-	-
SO	31	-	-	-	-	-	18.8	-	-	-	-	-	-
SO	38	-	-	-	-	-	-	-	17.7	-	-	-	-

Table 3

		t/δ_o				S_s(MeV)				S_c(Mev)			
Method	Ref	SI'	SIII	SkM	SkM*	SI'	SIII	SkM	SkM*	SI'	SIII	SkM	SkM*
Restricted variation with a Fermi function (RV1)													
TF	PW	1.00	0.90	1.51	1.52	-39.2	-36.1	-62.7	-61.7	-28.0	-31.7	-59	-59
						-30.2	-25.5	-41.3	-40.5	31	52	78	81
ETF1	PW	0.96	0.80	1.4	1.4	-38.9	-33.2	-58.9	-58.0	-27	-26	-51	-52
						-27.2	-22.0	-36	-36	41	50	84	88
ETF1+SO	PW	0.87	0.78	1.29	1.31	-34.8	-31.7	-52.4	-52.3	-21.7	-23.0	-43	-44
						-25.5	-21.8	-36.0	-35.6	20	33	51	55
ETF2	PW	1.03	0.86	1.5	1.5	-41.9	-35.6	-62.2	-61.1	-32	-30	-57	-59
						-28.9	-23.4	-39	-38	48	58	97	100
ETF2+SO	PW	0.94	0.83	1.38	1.39	-38.0	-34.2	-56.1	-55.7	-26.1	-26.8	-49	-50
						-26.9	-22.7	-37.7	-37.1	29	42	65	68
ETF2+SO	34	-	-	-	-	-	-30	-53	-	-	-	-	-
ETF3	PW	1.10	0.91	1.6	1.6	-44.5	-37.6	-65.1	-63.7	-36	-34	-63	-63
						-30.4	-24.5	-41	-39	55	65	108	111
ETF3+SO	PW	1.01	0.88	1.45	1.46	-40.8	-36.3	-59.3	-58.6	-30.1	-30.3	-55	-55
						-28.3	-23.7	-39.4	-38.6	36	49	77	79
ETF4+SO	15	-	1.00	1.48	-	-	-36.1	-54.7	-	-	23.4	23.7	-
Restricted variation with a Fermi function to a power (RV2)													
ETF1+SO	PW	0.95	0.82	1.36	1.37	-33.8	-29.6	-48.4	-48.0	-24	-24	-45	-46
						-32	-27	-46	-46	4	15	10	12
ETF2+SO	PW	1.06	0.92	1.50	1.51	-37.9	-32.7	-53.1	-52.2	-30	-30	-54	-55
						-36	-31	-51	-50	6	16	11	13
ETF3+SO	PW	1.17	1.00	1.62	1.62	-41.2	-35.4	-56.8	-55.8	-38	-36	-62	-62
						-40	-34	-56	-55	7	18	14	15
Restricted variation with a Fermi function to a power X Gaussian (RV3)													
ETF1+SO	29	-	-	-	-	-	-47.3	-	-	-	35.0	-	-
Exact variation													
TF	33	1.01	-	-	-	-36	-	-	-	-	-	-	-
ETF2+SO	34	-	-	-	-	-	-29	-53	-	-	-	-	-
Hartree-Fock													
no SO	39	-	-	-	-	-38	-	-	-	-	-	-	-
SO	31	-	1.16	-	-	-	-34	-	-	-	-	-	-

TABLE 4

Force	x	$\rho_N(fm^{-3})$	$\rho_B(fm^{-3})$	$-\Delta$
SI' TF	0.5	0.0655	0.0677	0.071
	0.3	0.0569	0.0593	0.105
	0.1	0.0609	0.0664	-0.025
ETF+SO	0.5	0.0612	0.0634	0.099
	0.3	0.0536	0.0562	0.127
	0.1	0.0661	0.0719	-0.069
SIII TF	0.5	0.0598	0.0620	0.081
	0.3	0.0554	0.0581	0.103
	0.1	0.0603	0.0736	0.007
ETF+SO	0.5	0.0566	0.0589	0.103
	0.3	0.0523	0.0551	0.124
	0.1	0.0623	0.0750	-0.005
SkM TF	0.5	0.0595	0.0617	0.122
	0.3	0.0485	0.0508	0.149
	0.1	-	-	-
ETF+SO	0.5	0.0558	0.0581	0.145
	0.3	0.0464	0.0488	0.164
	0.1	-	-	-
SkM* TF	0.5	0.0590	0.0613	0.125
	0.3	0.479	0.0503	0.155
	0.1	-	-	-
ETF+SO	0.5	0.0555	0.0578	0.147
	0.3	0.0456	0.0480	0.172
	0.1	-	-	-

TABLE 5

Force	A^{TF}	σ_s^{TF}	σ_c^{TF}	a^{TF}	A^{ETF}/A^{TF}	B	-C	σ_s^{ETF}	σ_c^{ETF}	a^{ETF}	κ
SI'	41.0	0.948	0.192	1.66	0.912	0.198	0.812	1.041	0.309	1.54	0.778
		0.924	0.181	1.69				1.034	0.296	1.61	
SIII	63.0	1.041	0.258	2.03	0.804	0.156	0.561	1.061	0.339	1.83	0.804
		1.020	0.246	2.06				1.074	0.339	1.93	
SkM	63.5	0.946	0.317	2.74	0.848	0.133	0.683	0.931	0.392	2.38	1.311
		1.020	0.356	2.61				1.059	0.452	2.34	
SkM*	68.2	0.981	0.340	2.84	0.859	0.123	0.628	0.968	0.416	2.49	1.311
		1.056	0.382	2.70				1.096	0.481	2.45	

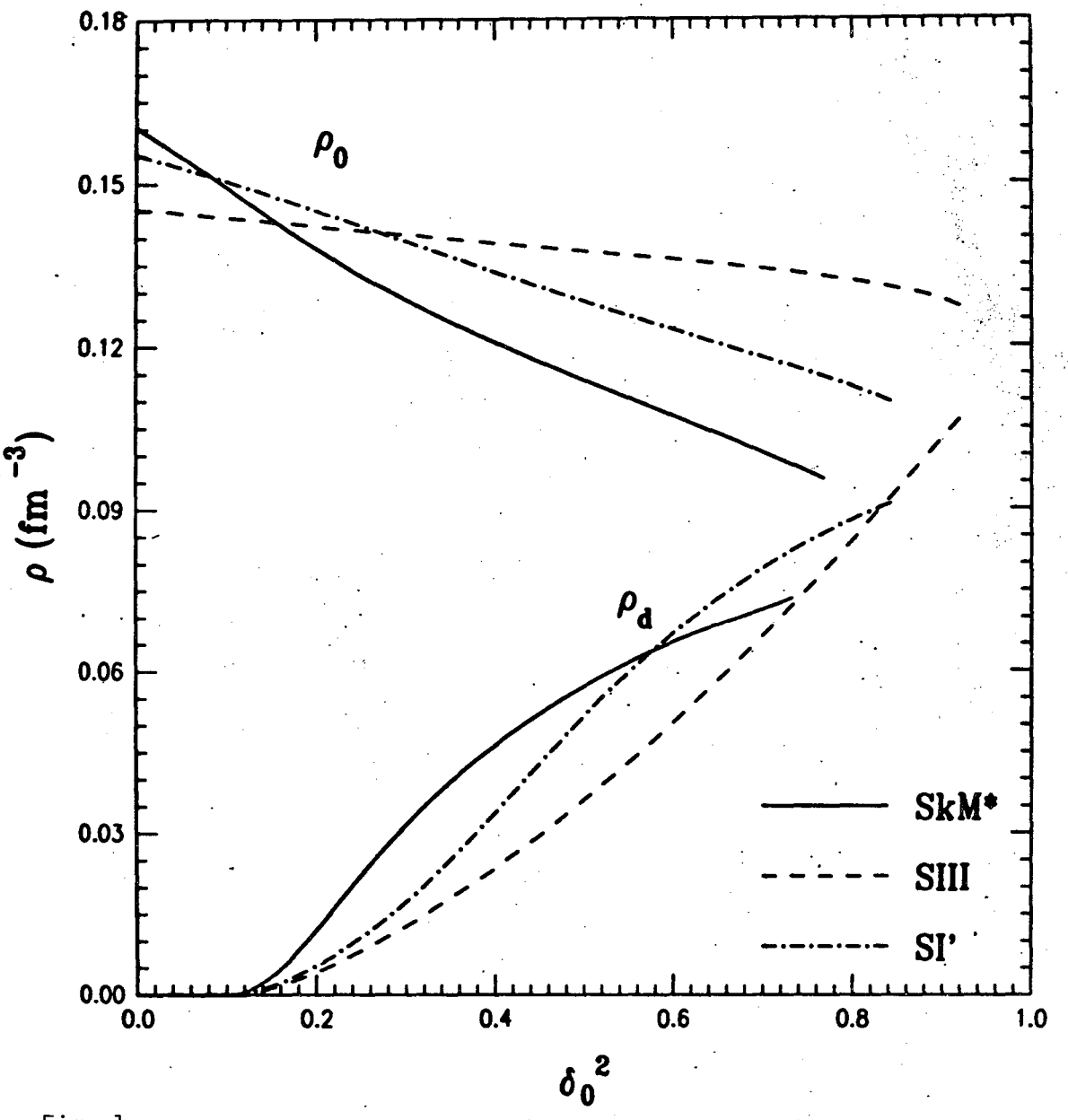

Fig. 1

XBL 848-3609

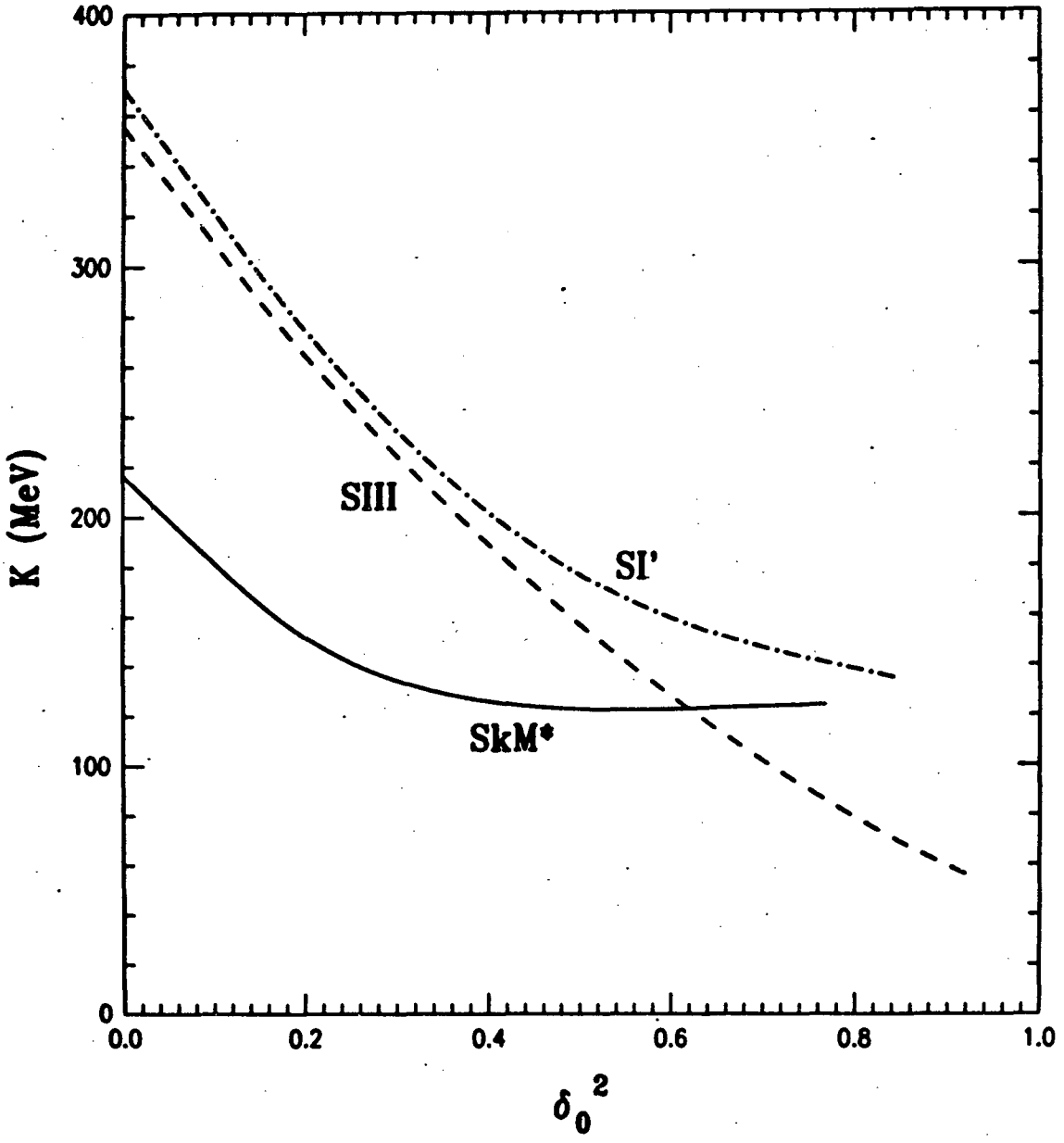

Fig. 2

XBL 848-3606

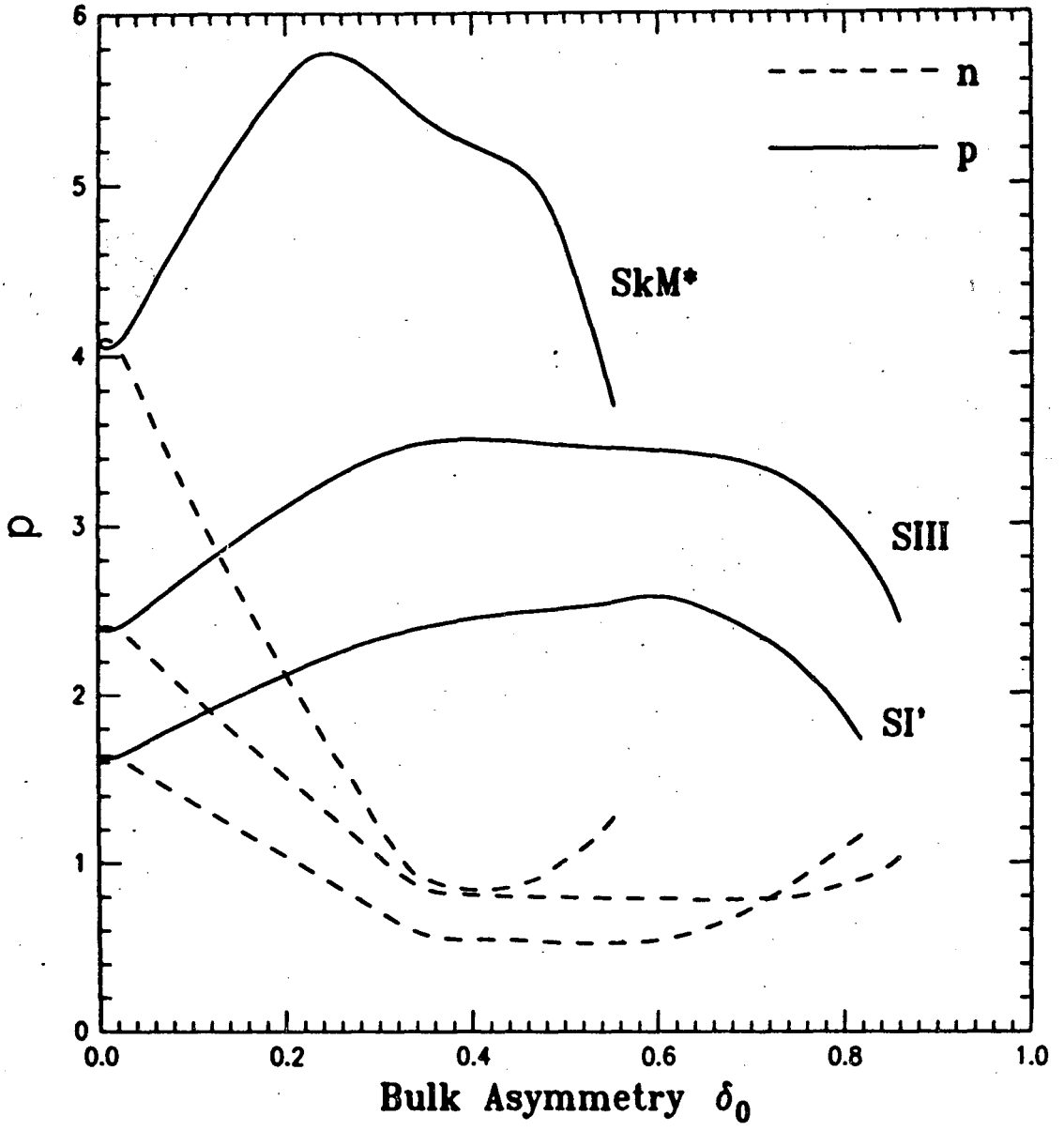

Fig. 3

XBL 848-3612

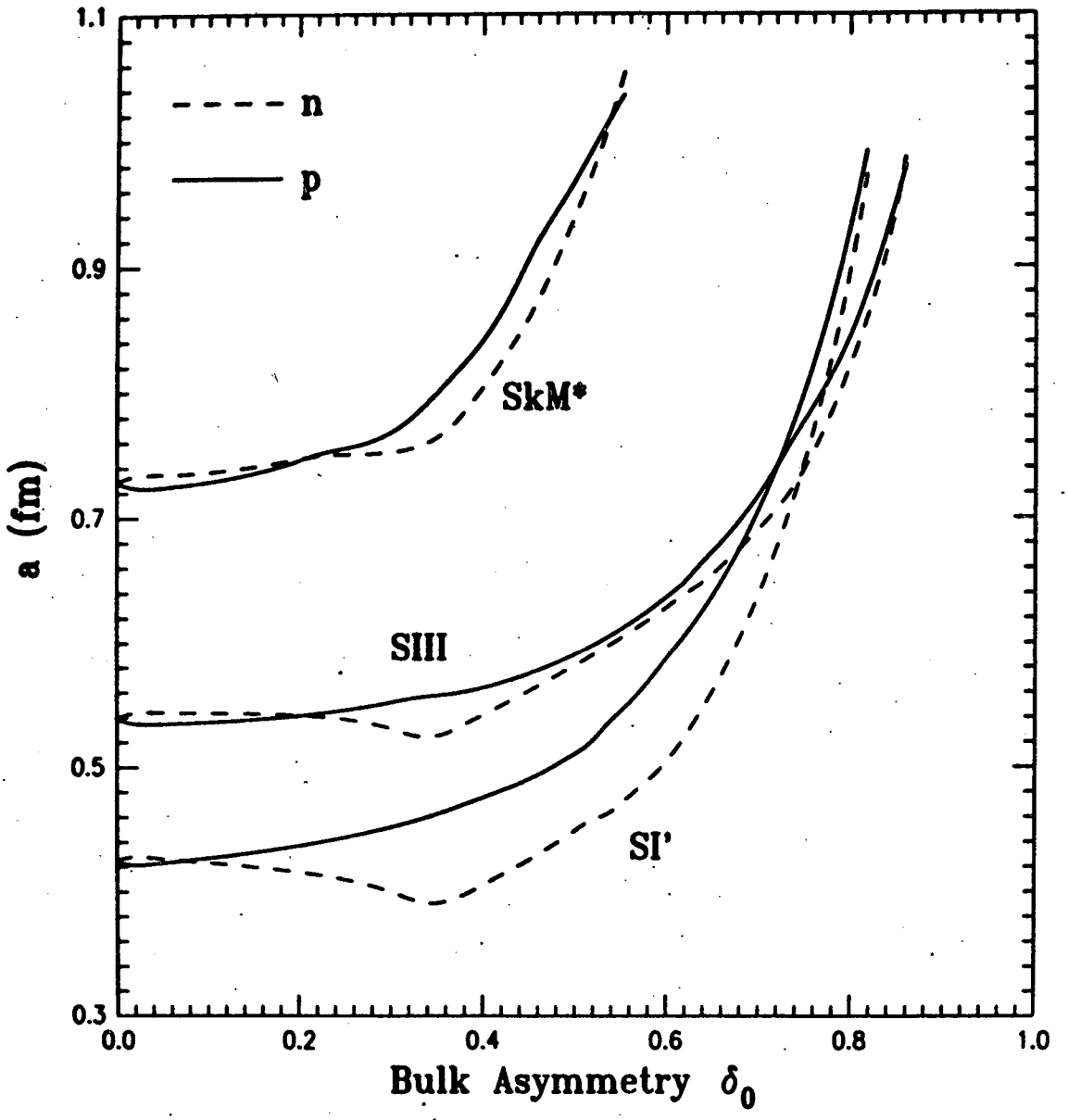

Fig. 4

XBL 848-3613

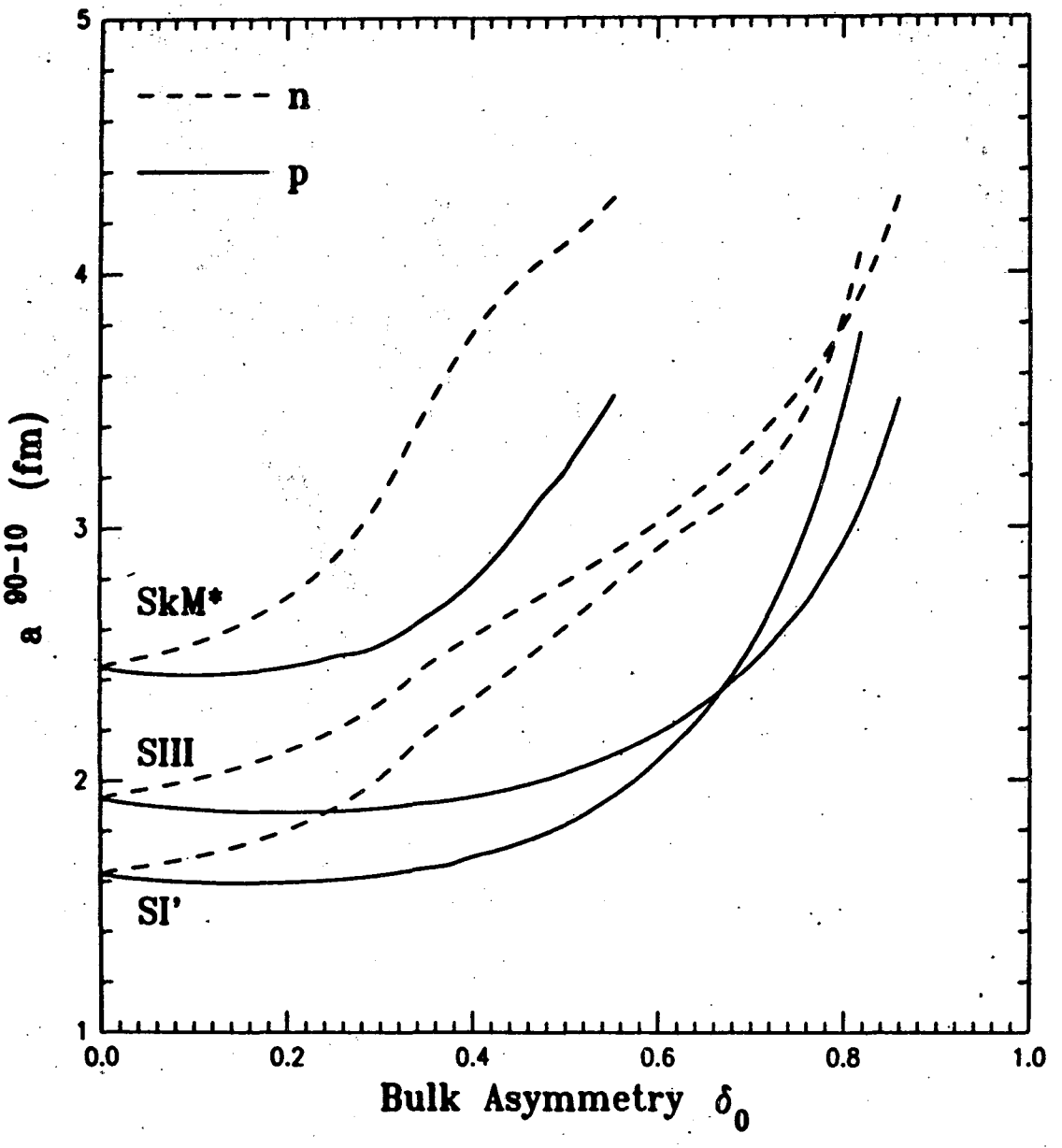

Fig. 5.

XBL 848-3611

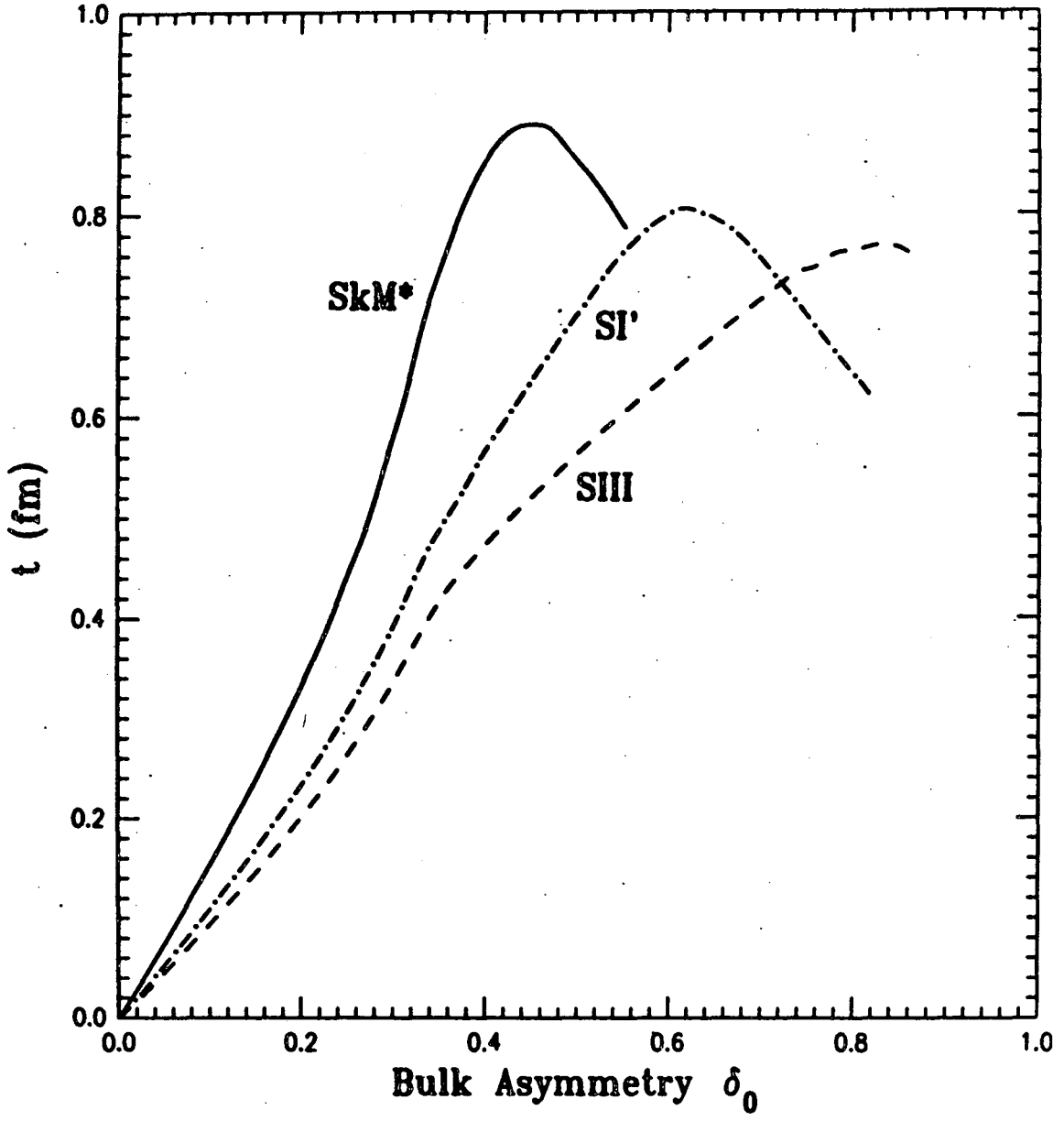

Fig. 6

XBL 848-3610

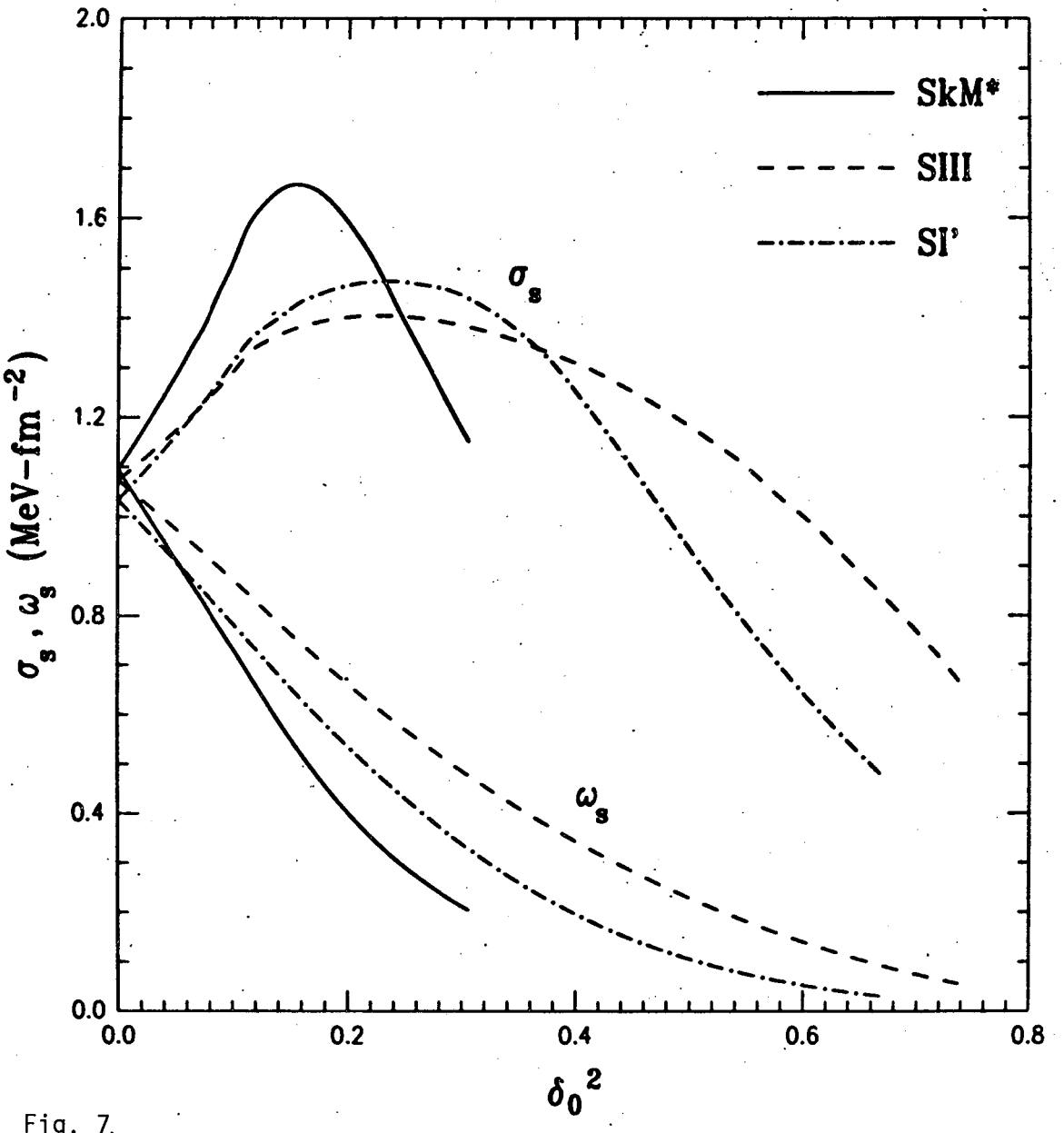

Fig. 7.

XBL 848-3607

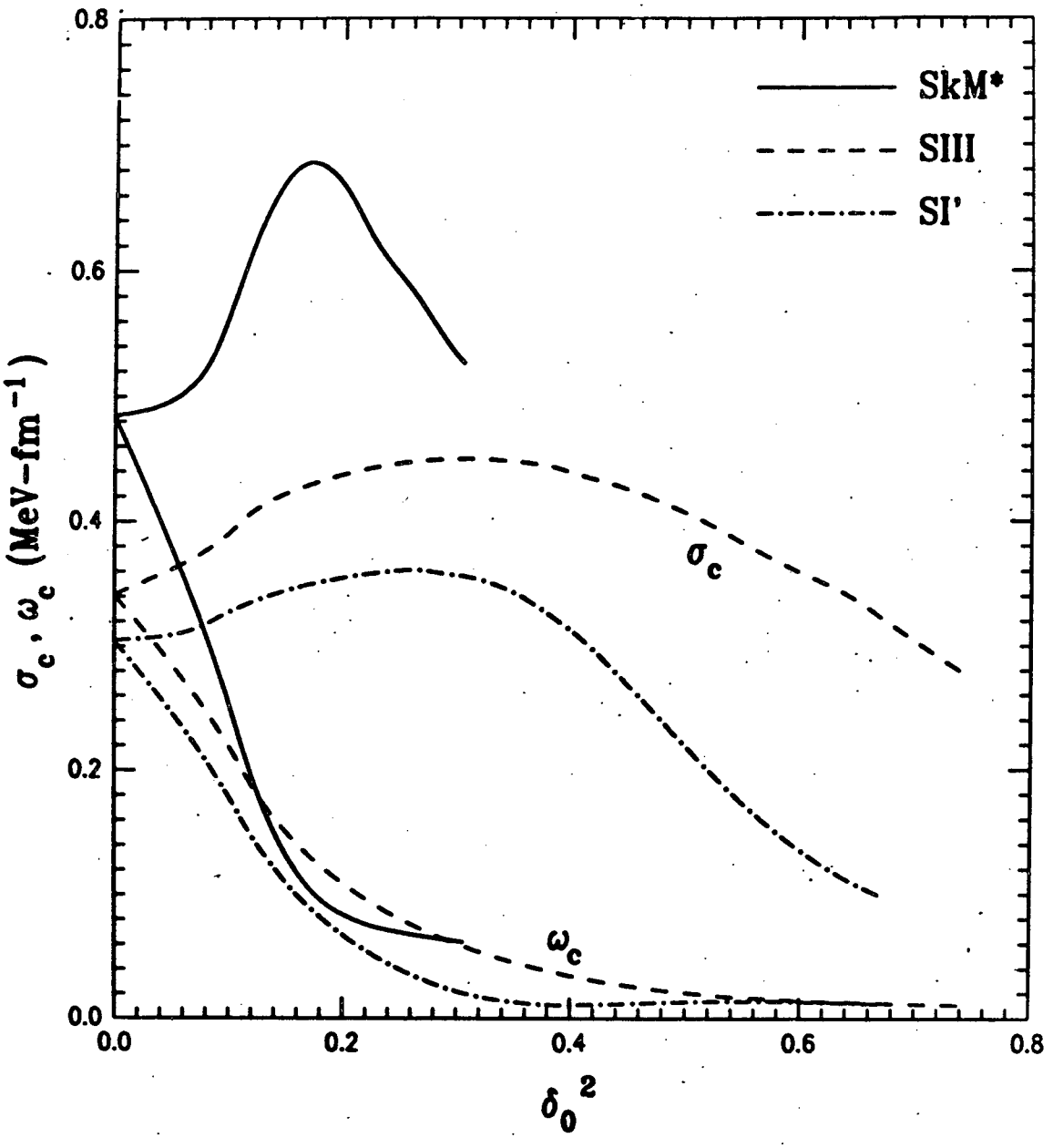

Fig. 8

XBL 848-3608

This report was done with support from the Department of Energy. Any conclusions or opinions expressed in this report represent solely those of the author(s) and not necessarily those of The Regents of the University of California, the Lawrence Berkeley Laboratory or the Department of Energy.

Reference to a company or product name does not imply approval or recommendation of the product by the University of California or the U.S. Department of Energy to the exclusion of others that may be suitable.

TECHNICAL INFORMATION DEPARTMENT
LAWRENCE BERKELEY LABORATORY
UNIVERSITY OF CALIFORNIA
BERKELEY, CALIFORNIA 94720